UNIVERSITÀ DEGLI STUDI DI TRIESTE

XXXI CICLO DEL DOTTORATO DI RICERCA IN

NANOTECNOLOGIE

AFM AS A TOOLBOX FOR ASSESSING THE MECHANICAL PROPERTIES OF CELLS WITH GENETIC MUTATIONS

Settore scientifico-disciplinare: ING-IND/22

DOTTORANDO / A
ILARIA PECORARI

COORDINATORE
PROF. LUCIA PASQUATO

SUPERVISORE DI TESI
PROF. ORFEO SBAIZERO

ANNO ACCADEMICO 2017/2018

Considerate la vostra semenza:
fatti non foste a viver come bruti,
ma per seguir virtute e canoscenza.

Consider well the seed that gave you birth:
you were not made to live your lives as brutes,
but to be followers of worth and knowledge.

(Dante Alighieri)

Index

ABSTRACT - 1 -

RIASSUNTO - 3 -

INTRODUCTION - 5 -

CHAPTER 1: CELL MECHANICS AND AFM - 7 -

1.1 Cell mechanics, or mechanobiology: that is the question - 7 -

1.2 Atomic force microscopy - 8 -

1.3 The imaging machine - 10 -
  1.3.1 Contact mode - 10 -
  1.3.2 Non-contact mode - 10 -
  1.3.4 Intermittent mode (tapping) - 10 -
  1.3.5 Applications of AFM imaging in biology - 11 -

1.4 The mechanical machine - 12 -
  1.4.1 Force-distance experiments - 13 -
  1.4.2 Fitting the F-d curves - 14 -

1.5 Measuring the stiffness by AFM - 15 -
  1.5.1 Who contributes to cell stiffness? - 18 -
    1.5.1.1 The cytoskeleton - 18 -
    1.5.1.2 The nucleus - 19 -

1.6 Measuring the adhesion by AFM - 20 -
  1.6.1 Who contributes to cell adhesion? - 23 -
    1.6.1.1 Desmosomes - 23 -

CHAPTER 2: THE GENETIC DISEASES - 27 -

2.1 Arrhythmogenic cardiomyopathy - 27 -
  2.1.1 Genetic background of AC - 29 -
    2.1.1.1 Genes coding for desmosomal proteins - 30 -
    2.1.1.2 Genes coding for nondesmosomal proteins - 30 -
  2.1.2 PKP2 at a glance - 31 -

2.2 Dilated cardiomyopathy - 32 -
  2.2.1 Genetic background of DCM - 33 -

2.2.2 FLNC at a glance - 33 -

2.3 Hutchinson-Gilford progeria syndrome **- 35 -**
2.3.1 Genetic background of HGPS and LMNA at a glance - 36 -

CHAPTER 3: MATERIALS AND METHODS - 41 -

3.1 Cell culture **- 41 -**
3.1.1 AC/*PKP2* framework - 41 -
3.1.2 DCM/*FLNC* framework - 41 -
3.1.3 HGPS/*LMNA* framework - 41 -

3.2 Infection of NRCFs, JRCFs, and ARCFs with adenoviral vectors **- 42 -**

3.3 Immunofluorescence experiments **- 42 -**

3.4 AFM sample preparation **- 43 -**
3.4.1 AC/*PKP2* framework - 43 -
3.4.2 DCM/*FLNC* framework - 43 -
3.4.3 HGPS/*LMNA* framework - 43 -

3.5 AFM experiments **- 44 -**
3.5.1 AC/*PKP2* framework - 44 -
3.5.2 DCM/*FLNC* framework - 44 -
3.5.3 HGPS/*LMNA* framework - 45 -

3.6 Stiffness and adhesion data analysis **- 46 -**

3.7 Nuclear shape descriptor (circularity) assessment **- 47 -**

3.8 Statistical analyses **- 47 -**

CHAPTER 4: RESULTS AND DISCUSSION - 49 -

4.1 AC/*PKP2* framework **- 49 -**
4.1.1 Stiffness - 49 -
4.1.2 Adhesion - 50 -

4.2 DCM/*FLNC* framework **- 51 -**
4.2.1 Stiffness - 51 -
4.2.2 Adhesion - 53 -

4.3 HGPS/*LMNA* framework **- 54 -**
4.3.1 Stiffness - 55 -
4.3.2 Adhesion - 57 -

CHAPTER 5: CONCLUSIONS - 59 -

BIBLIOGRAPHY - 63 -

ACKNOWLEDGEMENTS - 81 -

Abstract

Most diseases are being found to have a genetic component, which most likely triggers a cascade of events and eventually affects the overall cell mechanical properties. Over the years, the mechanical characteristics of cells have raised a great interest in the scientific community, since cells have been shown to play a key structural role in building complex structures like tissues and organs, and are able to sense, transduce and exert forces on their surroundings. Among the numerous techniques developed to study cell mechanics, atomic force microscopy (AFM) has often proven to be effective in discerning cell mechanical properties in health and disease.

This work aimed to show the power of AFM in the study of cell mechanics under the effect of genetic mutations. To assess the versatility of AFM technique, this thesis contemplated three genetic diseases, and likewise genes. Specifically, the present study focused on arrhythmogenic cardiomyopathy (AC) and *PKP2* gene, dilated cardiomyopathy (DCM) and *FLNC* gene, Hutchinson-Gilford progeria syndrome (HGPS) and *LMNA* gene. Despite being genetically and phenotypically different, all the aforementioned diseases affect the heart, which was therefore chosen as the target of this work.

Either gene suppression or mutation were induced in cardiac cells, which were then probed by AFM to assess their mechanical properties. *PKP2* was knocked down in HL-1 cells by shRNA targeting; CRISPR/Cas9 was applied to knock out *FLNC* in human induced pluripotent stem cells (hiPSC), then differentiated into cardiomyocytes; and a mutant form of *LMNA*, known to cause HGPS, was expressed in primary rat cardiac fibroblasts using an adenoviral vector. Rat cardiac fibroblasts were isolated from neonatal, juvenile, and adult animals.

PKP2-deficient HL-1 cells and mutant juvenile rat cardiac fibroblasts exhibited altered mechanical properties compared to controls, whereas no variation in the mechanical behaviour was detected in all the other samples. A relationship between variation of cell stiffness and alteration of the distance at which the maximum adhesion force occurs was discovered. These results demonstrated that AFM is a powerful toolbox to study certain mechanical aspects in *in vitro* models of genetic diseases. Although, consideration may want to be given to some critical issues that had emerged, like the choice of an appropriate experimental setup and the cellular region to be investigated.

In conclusion, this study should encourage more researchers to address biological questions from a mechanical point of view, since biomechanical properties can be identified as potential targets for novel medical approaches.

Riassunto

Al giorno d'oggi, è ormai noto che la maggior parte delle malattie possiede una componente genetica, la quale può potenzialmente innescare una cascata di eventi ed avere come risultato finale un'alterazione delle proprietà meccaniche cellulari. Queste ultime hanno considerevolmente attratto l'attenzione della comunità scientifica, la quale ha preso coscienza del ruolo strutturale delle cellule in organi e tessuti e della capacità delle cellule stesse di captare, trasdurre ed esercitare forze sull'ambiente circostante. Tra i metodi sviluppati per lo studio della meccanica cellulare, la microscopia a forza atomica (AFM) si è ripetutamente dimostrata efficace nel discernere il comportamento meccanico delle cellule in condizioni fisiologiche e patologiche.

Il presente lavoro di tesi si propone di illustrare le potenzialità dell'AFM nello studio delle proprietà meccaniche di cellule in modelli *in vitro* di malattie genetiche. Per avvalorare la versatilità della tecnica, sono state prese in considerazione tre malattie genetiche, ed altrettanti geni ad esse associati: nello specifico, la cardiomiopatia aritmogena ed il gene *PKP2*, la cardiomiopatia dilatativa ed il gene *FLNC*, e la sindrome di Hutchinson-Gilford (detta anche progeria) ed il gene *LMNA*. Nonostante siano genotipicamente e fenotipicamente diverse, le suddette malattie condividono un aspetto comune: tutte e tre, infatti, hanno effetti di variabile intensità sul cuore, il quale è stato pertanto scelto come oggetto di studio della tesi.

In alcuni tipi cellulari cardiaci sono state indotte la soppressione o la mutazione dei geni sopra citati: ad esempio, nelle cellule HL-1, ovvero una linea cellulare rappresentativa del muscolo cardiaco, è stato introdotto un meccanismo shRNA per silenziare *PKP2*. Il gene *FLNC*, invece, è stato modificato tramite CRISPR/Cas9 in cellule staminali (hiPSC) che sono state successivamente differenziate in cardiomiociti. Per lo studio della progeria, infine, fibroblasti cardiaci primari di ratto in età neonatale, giovane ed adulta sono stati infettati con un vettore adenovirale che esprimeva la proteina LMNA in forma *wild-type* o mutata. Ogni tipo cellulare, con la rispettiva mutazione genetica, è stato poi studiato con l'AFM.

Nelle cellule HL-1 con *PKP2* soppresso e nei fibroblasti da ratto giovane con LMNA mutata sono state riscontrate variazioni delle proprietà meccaniche, mentre negli altri campioni non è stato rilevato alcun cambiamento. In particolare, laddove sono state misurate differenze nelle proprietà meccaniche di controlli e mutanti, i parametri soggetti a variazione erano sempre gli stessi, ovvero il modulo di Young e la distanza a cui si manifestava la massima forza di adesione. Parrebbe dunque esservi una relazione tra queste due proprietà, ovvero all'aumentare di una, l'altra diminuisce, e viceversa.

I risultati ottenuti dimostrano inequivocabilmente che l'AFM può essere considerata una tecnica di elezione anche nello studio delle caratteristiche meccaniche di modelli *in vitro* per malattie genetiche. Nonostante ciò, bisogna sempre tenere in considerazione le potenziali criticità che questo lavoro ha messo in luce, come ad esempio la necessità di scegliere in modo appropriato il setup sperimentale, nonché la regione della cellula da sottoporre ad indagine.

In conclusione, questa tesi dovrebbe incoraggiare sempre più ricercatori ad intraprendere lo studio delle proprietà meccaniche di una cellula, in modo tale che in un futuro, sperabilmente non lontano, esse possano diventare il target di approcci clinici innovativi.

Introduction

"In nature we never see anything isolated, but everything in connection with something else which is before it, beside it, under it and over it."
This quote from Johann Wolfgang von Goethe can be easily applied to every living organism, including but not limited to cells. Cells are not isolated units, but interact with other cells and the surrounding environment. Among the plethora of exchanges that can take place, cells are able to sense mechanical cues from the surroundings and exert forces on their neighbourhoods. Cells are the building blocks of more complex structures (tissues and organs), so they play a structural role that cannot be ignored. It should be clear that the study of a biological problem cannot exclude mechanical characteristics, whether it is a cell structural property or the mechanisms by which cells sense and transduce mechanical signals. This concept calls for methods to assess and quantify mechanical phenomena in cells and tissues.

Atomic force microscopy (AFM) was introduced in middle 1980s, as a new method to investigate material properties at very small scales. It was but a short step from surfaces of insulators to biological samples. Over the years, AFM has become a routine technique in biology, and has proven to be effective in discerning the mechanical behaviour of cells in health and disease. Nevertheless, it is obvious that AFM cannot entirely describe a pathologic phenotype. The "*macro*" aspects, as the outcomes for the patients, can be tackled only by physicians, whereas the "*nano*" features are matter for molecular biologists. AFM can assess the "*meso*"-world, providing useful insights into cell mechanics, and then bridging what has been observed by the specialists of the other "scales".

In this thesis, we aim to show the power of AFM in studying *in vitro* models of genetic diseases. Most diseases have been demonstrated to bear a genetic component, which may trigger a cascade of events and affect the mechanical behaviour of a cell. In order to show the versatility of AFM, we studied three genetic diseases: arrhythmogenic cardiomyopathy (AC) with *PKP2*, dilated cardiomyopathy (DCM) with *FLNC*, and Hutchinson-Gilford progeria syndrome (HGPS) with *LMNA*. Although these diseases are genetically and phenotypically different, they all affect the heart, which was therefore chosen as the focus of this work. We exploited various methods to induce genetic mutations and we tested different cell types.

In Chapter 1, we discuss the importance of cell mechanics, and explain AFM techniques and modes of operation. We present the mechanical properties that can be measured by AFM and highlight the cell components that contribute the most to these mechanical aspects.

In Chapter 2, AC, DCM, and HGPS are described, particularly in relation to the specific mutations studied, i.e. *PKP2*, *FLNC*, and *LMNA*.
Chapter 3 is dedicated to the materials and methods used in the present work.
Chapter 4 reports the results achieved and discussion.
Chapter 5 concludes the work, summarising the relevant findings with suggestions for future work.

Chapter 1: Cell mechanics and AFM

The observation of physical and mechanical phenomena in living organisms is not a recent discovery. Wilhelm His proposed the idea that cells are subjected to the laws of physics in 19th century, when also Julius Wolff postulated his famous law on bone remodeling [1,2].

Physics and mechanics were thought to be related to life, but any effort in this field was unfortunately torn apart. Proper technologies that could have tested and confirmed any hypotheses were lacking. The scientific interest was therefore focused on unraveling molecular and genetic mechanisms.

The advent of sophisticated tools and nanotechnologies called again the attention of academics to the role played by physical events in biology. A new era started then: mechanobiology and biomechanics showed up as a rapidly growing field of study.

1.1 Cell mechanics, or mechanobiology: that is the question

Living organisms and cells are not isolated units: they interact, they sense, and they respond to what they perceive. A type of cell response is **mechanotransduction**: the cell senses a physical stimulus, like a force, and converts it into a signal of different nature, like electrical or chemical.

Mechanobiology is the discipline that studies the effects induced by physical cues on living systems, at any scale: hence, it studies also the mechanotransduction. Mechanobiology is often overlapped with biomechanics, but there might be distinct differences. Biomechanics is the study of structural and mechanical properties of a living system, and when the living system under investigation is a cell, it is termed **cell mechanics**. That begs the questions: where should we focus our efforts? Cell mechanics or mechanobiology? The answer is quite simple, since the two are mutually dependent. Indeed, cell mechanical properties are crucial for mechanotransduction mechanisms, and mechanotransduction can trigger changes in the cell mechanical properties.

Notably, experimental procedures are usually directed to either mechanobiology or cell mechanics; ergo, they need to be integrated with other techniques to entirely describe a phenomenon.

We will now have a look at few examples in mechanobiology and cell mechanics, trying to raise the interest of the reader in these fields and convince him/her about the relevance of this type of studies.

One of the hottest trends in science is certainly the study of stem cells, because of their ability to differentiate towards different cell type and their potentialities in regenerative/reparative medicine. Researchers have discovered that mechanical aspects cannot be ignored when dealing with stem cells. Indeed, these cells are largely influenced by the stiffness of the surrounding environment, namely cells exhibit different behaviours as they sense either a soft or stiff substrate. Engler et al. demonstrated that human mesenchymal stem cells (MSCs) respond to substrate stiffness, differentiating into various lineages: soft matrices are neurogenic, whereas stiffer matrices are either myogenic or osteogenic [3]. Osteogenic differentiation has been observed also on stiff substrates in human periodontal ligament stem cells (PDLSCs) [4]. Conversely, muscle stem cells (MuSCs) retained their "stemness" and their regenerative potential when cultured on compliant substrates [5].

Another relevant theme that captivates major efforts in the scientific community is cancer, which is the second leading cause of death worldwide, and has a huge economic impact (around 1.16 trillion USD in 2010) [6]. Despite the many progresses made so far, cancer remains an issue. Biomechanics is playing a pivotal role in revealing the mysteries of cancer. In particular, cell mechanics techniques showed that cancer cells, especially the highly invasive ones, are more deformable than controls [7]. This is potentially important to explain the mechanisms of cancer progression, since metastatic cells must be very deformable to intra- and extravasate, survive the blood stream, and invade other sites [7]. This information needs to be complemented by other experiments (e.g. directed to the molecular mechanisms). Nonetheless, these results could eventually lead to identify mechanical features as therapeutic targets, which is one of the key goals for researchers in the field.

After this introductive section, the focus is now pointed to atomic force microscopy (AFM), one of the techniques that contributed the most to the success of cell mechanics.

1.2 Atomic force microscopy

In 1986, Binnig, Quate and Gerber published a groundbreaking work, describing a new microscope that was able to investigate surfaces of insulators at the atomic scale [8]. Their invention, the atomic force microscope, paved the way for studying the structure of matter at a different level.

AFM is part of the broader family of scanning probe microscopies (SPM), in which a physical probe scans and images a specimen. The working principle of AFM and SPM can be easily understood from the following analogy: a blindfolded person cannot see the surrounding environment, so needs a stick to locate the objects around. The stick allows to "shape" the objects and sense their deformability, that is if they are soft or stiff.

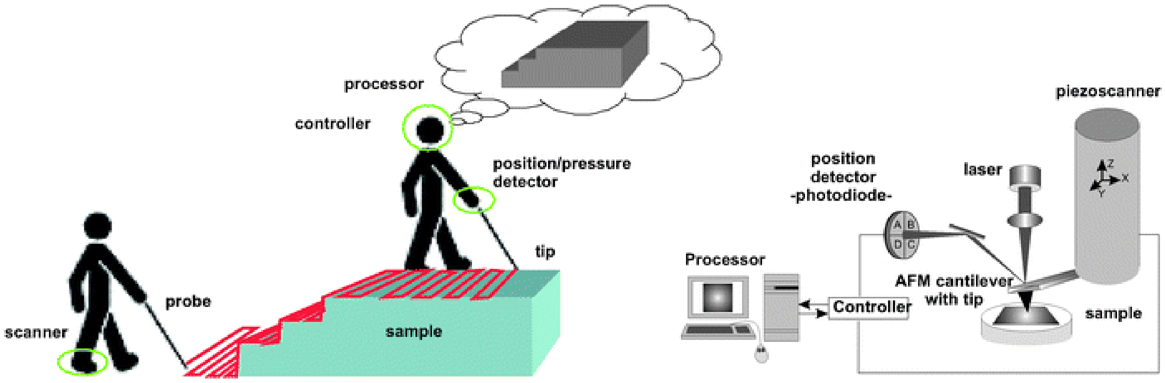

Figure 1 Similarities between AFM and blind inspection of objects [9].

In AFM, the "stick" is like a record player's arm (i.e. the cantilever) with a stylus at one of its edges (i.e. the AFM tip). A laser beam is reflected off the cantilever surface and collected by a matrix of photodiodes. Whenever the tip interacts with a sample, the cantilever bends, and the deflection is detected as a variation of the currents transduced by the photodiodes. Driven by a piezoelectric scanner, the cantilever-tip system scans the specimen in the xy plane, meanwhile the vertical position of the sample is monitored.

The characteristics of the cantilever-tip assembly, like material and shape, strongly depend upon the application. Silicon (Si) and silicon nitride (Si_3N_4) are a common choice, with the latter usually softer than the former [10]. Silicon nitride cantilevers are often coated with gold, in order to enhance their reflectivity; unfortunately, the cantilevers thus manufactured are more sensitive to small temperature drifts [10]. Nonetheless, the gold coating has proven to be convenient when the cantilever-tip assemblies have to be functionalised with certain groups or proteins of interest. The cantilever-tip functionalisation is required for some chemical and biological applications, and gold allows exploiting the thiol-gold chemistry.

Cantilevers and tips can be made out of distinct materials. For instance, CP-PNP-SiO probes (NanoAndMore Gmbh) have a Si_3N_4 cantilever, but the spherical tip is made of silicon dioxide (SiO_2). Both tip and cantilever may have various shape and geometries (e.g. sphere and cone for the tip, triangle or rectangle for the cantilever).

Theoretically, AFM probe customisations are endless, and tip-cantilever systems may be tailored depending on the specific application. In particular, consideration may want to be given to the mode in which the AFM will operate, the environment and the type of specimen.

Over the years, it has been demonstrated that atomic force microscopy is a versatile technique, ranging from surface imaging to probing mechanical properties. According to Benitez and Toca-Herrera, AFM can be either an imaging or a mechanical machine [11]. In the following sections, both aspects will be described.

1.3 The imaging machine

When used as an imaging tool, the AFM modes of operation depend upon the nature of the forces acting between AFM tip and sample, namely attractive or repulsive. When tip and specimen are very close, their atomic orbitals overlap and a repulsive force occurs (e.g. because of Pauli repulsion phenomenon). Vice versa, an attractive force appears whenever the distance between AFM probe and sample is greater.

The main operating modes are: contact (repulsive forces), non-contact (attractive forces), and intermittent ("hybrid" between contact and non-contact).

1.3.1 Contact mode

The tip is in contact with the sample, and the repulsive forces cause the deflection of the cantilever according to the specimen profile. Contact mode is usually classified in two sub-modes: constant force and constant height. In constant force mode, the cantilever deflection is kept constant, while the probe moves in the z-direction. In constant height mode, the tip is always at a fixed height above the specimen, and the cantilever deflection is directly measured.

Lateral force microscopy is also a type of contact mode, but instead of measuring the z-deflection, the lateral deflection is recorded.

Contact mode can be quite "rough" on the sample, because of the relatively high lateral forces between tip and specimen. These might result in sample/tip damage or movement of entities that are loosely attached to the sample surface.

1.3.2 Non-contact mode

Martin et al. introduced this mode, exploiting the tip-sample spacing for profiling the specimen under investigation [12]. In this mode, the tip is slightly above the sample (in the order of tens, hundreds of angstroms), and the forces between AFM probe and specimen are therefore attractive. As the cantilever oscillates, the tip scans the specimen surface.

In non-contact mode, it is pivotal - but challenging - to maintain constant the tip-sample separation and prevent the probe from contacting the specimen. If the tip-sample contact accidentally occurs, the tip could eventually stick to the specimen surface.

1.3.4 Intermittent mode (tapping)

In this mode, the cantilever oscillates at, or close to, its resonant frequency, and the tip intermittently taps the sample surface. Tapping mode trespasses the attractive and repulsive regimen of forces. The resonance depends on the geometry and material properties of the cantilever [13].

One particular tapping mode is amplitude modulation. Here, when the tip touches the specimen, the amplitude of oscillation is reduced by the energy lost in the contact. As soon as the tip is moved away from the specimen, the amplitude of oscillation increases again. These variations allow the detection of surface characteristics.

Intermittent mode is often chosen because lateral forces are ideally zeroed, so lateral resolution is enhanced. Tapping mode minimises the tip-sample degradation, since the contact between them is discontinued. Despite these advantages, the user should be aware that intermittent mode can be critical when samples are analysed in acqueous environments. In fact, liquids can induce damping effects on the cantilever oscillation, which might result in a challenging choice of the peak of resonance [13]. These issues need to be considered, but do not prevent the use of intermittent mode for imaging samples in liquid.

1.3.5 Applications of AFM imaging in biology

Since the AFM can work in liquid environments and at subnanometre scale, it was early expected to address biological questions. Over time, the wide field of biology has been widely explored by AFM imaging, ranging from nucleic acids, to viruses, bacteria, mammalian cells and tissues.

In early 1990s, AFM imaging of DNA raised a great interest among the microscopists, leading to the rapid development of more and more accurate methods. By way of example, in 1993 Hansma et al. described reliable procedures to image double- and triple-stranded DNA, single-stranded RNA homopolymers, and more interestingly, single-stranded DNA 25 bases short [14]. The reader can find a comprehensive overview of AFM imaging and DNA in the works of Hansma et al. and Lyubchenko et al. [15,16].

Thanks to its peculiarities, AFM imaging successfully revealed the structural features of viruses. For instance, Kuznetsov and colleagues used AFM to show both surface and internal structures of human immunodeficiency and murine leukemia viruses [17]. Over the years, the technique has been consistently improved, e.g. frequency modulation atomic force microscopy was exploited to observe the configuration of parvovirus minute virus of mice at high resolution [18]. A broader perspective of this field is offered in the work of Kuznetsov and McPherson [19].

AFM imaging met with success with bacteria. An interesting application was the study of the bacterium-material interactions, done by Dubrovin et al. [20]. Moreover, AFM studies proved to be useful in monitoring the influence of certain biofilm components on the morphology of *Salmonella* Typhimurium [21]. Other examples are partially reported in the paper of Dufrene [22].

AFM imaging was largely used to characterise certain processes in mammalian cells, like endo- and exocytosis. Hecht and colleagues observed the exocytosis of lamellar bodies, resulting in an increase of height/volume of lung epithelial cells [23]. On the other hand, clathrin-mediated endocytosis in COS-7 cells caused morphological variations in the plasma membrane, as easily detected by AFM [24]. Another process, the locomotion, was investigated by Li et al. in MCF-7 and Neuro-2a cells [25]. Since AFM technique is very versatile, it was used even for more specific events, like fibrillogenesis. Indeed, in rat embryonic firboblasts (REF52), AFM imaged the initial stages of the formation of large fibrillar networks from fibronectin [26]. Lastly, AFM was exploited for detecting the effects of certain drugs on mammalian cells, as reviewed by Li and coworkers [27]. Further applications of AFM as an imaging tool for cells can be found in one of our paper [28].

It is worth mentioning that AFM was applied for studying the ultrastructural characteristics of larger samples, like tissues. For example, AFM shed light on fine structures in either intact or fractured trabecular bone [29]. Human aortic walls harvested with heart surgery were analysed by AFM and scanning electron microscopy [30], whereas Raman spectroscopy and AFM identified lipid raft clusters in endothelium of the aorta of a murine model for type 2 diabetes [31]. AFM imaging applications on tissue sections derived from different body sites are depicted in the paper of Graham et al. [32].

To conclude this section, consideration may want to be given to the application of AFM imaging on cardiac samples, specifically cells, as this is a key aspect of the present work. For instance, Yang and colleagues investigated the mechanisms of internalisation and transmembrane transport of a synthetic polypeptide (GCIP-27) in cardiac cells. By using AFM, authors found a significant increase in the surface roughness of neonatal rat cardiomyocytes, when administrated with GCIP-27 [33]. A variation of cell surface roughness was detected even in neonatal mouse cardiomyocytes treated with aldosterone, as they were found to be more irregular than controls [34]. Myocardial infarction (MI) was proven to dramatically change the surface properties of cardiomyocytes: indeed, the crest/hollow organisation, typical of adult murine cardiomyocytes, was compromised after MI [35]. Subcellular components, specifically the cytoskeleton, were investigated by AFM in neonatal mouse cardiomyocytes exposed to lipopolysaccharide (LPS), which is known to cause sepsis and cardiac dysfunction. LPS treatment showed to reduce the cytoskeletal density and increase cytoskeletal volume, thus leading to the conclusion that LPS causes the reorganisation of cardiomyocyte cytoskeleton [36].

1.4 The mechanical machine

AFM has been playing a pivotal role in mechanobiology/biomechanics mainly because of its ability to work in force spectroscopy mode. Force spectroscopy mode is a collection of procedures that are able to quantify the mechanical properties of a sample and the interactions between sample and tip.

Since there is no interaction between matter and radiation, the use of term "spectroscopy" could appear slightly inappropriate, but this denomination is so far well-established [37].

1.4.1 Force-distance experiments

At the beginning of a force-distance experiment, the cantilever-tip assembly is not in contact with the sample. The probe is moved toward the specimen until the contact occurs, the tip exerts a certain force, and penetrates/indents the sample. Afterwards, tip and cantilever are retracted from the sample, until the contact is lost. The contact period is termed dwell time [38].

These experiments usually result in the plot of cantilever deflection against the movement of the piezoelectric scanner (i.e. a distance). These plots are commonly known as force-distance (F-d) curves.

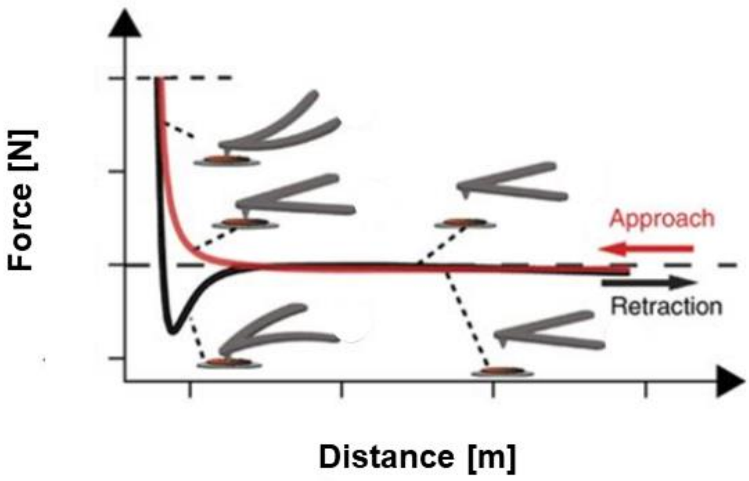

Figure 2 *Typical F-d curve. In the approach segment (red), the tip is moved toward the sample and indents it. During the retraction segment (black), the tip is retracted from the specimen until the contact is lost and the force value returns to zero. This picture is a modified version of [39].*

The mechanical properties of a sample are inferred from F-d curves. Generally, if the dwell time is null, the user can measure both stiffness (usually in terms of Young's modulus) and adhesive properties. Otherwise, stress relaxation and creep compliance can be assessed. A more detailed overview of stiffness and adhesion of cells measured by AFM will be given later in the text.

Performing F-d experiments on single cells can be challenging, and several precautions must be considered. For instance, if the cantilever is stiff, the deflection might be difficult to detect, whereas if it too soft, thermal vibrations could overlap the F-d curve or the indentation might not be adequate to reliably estimate mechanical properties [40].

When evaluating cell stiffness, consideration may want to be given to the followings.

- The intrinsic viscoelastic behaviour of a cell must always be taken into account. The tip has to be moved slowly against the sample (low indentation speed), in order to reduce the hydrodynamic/viscous contributes [41]. A typical range of indentation speeds is 50 nm/s ÷ 10 µm/s [11].
- Living cells adhered to a substrate like petri dish or coverslip can be modelled as thin layers on hard substrates. The indentation must be within 10% of the cell height to lower the hard substrate contribute [40]. This represents a challenge when probing peripheral areas of the cell, where the sample thickness is low.
- The stiffness is commonly calculated in terms of Young's modulus by fitting the F-d curves with an appropriate contact mechanics model. The most used is the Hertz model, but it implies two main assumptions: the indenter must have a parabolic shape, and the sample under investigation is very much thicker than the indentation depth [42].
- When comparing the stiffness of identical cell types, the shape of the indenter is crucial. Indeed, it has been shown that cells appear softer when probed by spherical indenters as opposed to conical ones [43].

1.4.2 Fitting the F-d curves

The raw data must be processed in order to get information about the mechanical properties. The case of stiffness is discussed here in detail.

First, the user should be aware that the x-axis in F-d curves has to be converted in the actual value of sample indentation, which is required in contact mechanics models (like Hertz model), for estimating the stiffness in terms of Young's/elastic modulus. As previously mentioned, the AFM software records the movement of the piezoscanner. However, when the probe penetrates the specimen, the cantilever deflects of a certain amount in the direction opposite to indentation. Hence, the sample is indented by a quantity that equals the piezoscanner movement minus the cantilever deflection caused by the penetration.

Then, the y-axis must be manipulated. The cantilever deflection is recorded from the photodiode matrix, therefore is expressed in either volts or amperes. Some preliminary calibration steps must be undertaken before applying the Hooke's law (that will convert the cantilever deflection into a force). The variation in photodiode signal has to be related with the distance that the cantilever actually deflects, so the photodiode output must be converted into a [m] value. This is done by assessing the sensitivity of the system. Practically, this conversion factor is obtained performing F-d experiments on a bare surface, much stiffer than the cantilever (thus the bare surface can be considered not deformable). The sensitivity is calculated from the contact region of the F-d curve so measured.

The cantilever spring constant is also required for computing Young's modulus, and can be assessed choosing among different methods, mainly based on beam or resonance theory.

The resulting curve displays force versus indentation and can be finally fitted with the model to estimate the Young's modulus.

1.5 Measuring the stiffness by AFM

At the beginning of this paragraph, it is crucial to introduce the concepts of stiffness and elasticity.

In materials science and engineering, the Young's/elastic modulus is an index of the stiffness of a material. Briefly, Young's modulus represents the ability of a material to withstand a deformation when subjected to either compression or tension.

In the AFM field, Young's modulus is also an index of the material stiffness. In particular, if we think about a cell, the stiffness represents the deformability, thus the ability to deform, of the cell itself. Hence, if a cell is softer than others (it has lower Young's modulus), will be more prone to deform and, e.g., squeeze.

Now, the question is: "**why should we investigate the stiffness of a cell, and how?**" For the first part, the answer is exhaustively given by Martin Y.M. Chiang and his co-authors:

"The impact of cell modulus (the deformability of cells or resistance to morphological change) extends beyond knowledge of a mechanical property to include cellular processes important in developmental biology, pathology, molecular biology, etc., as well as cell-material interactions in tissue engineering and regenerative medicine"[44].

Regarding the techniques used to quantify the cell stiffness, we will pass over micropipette aspiration, optical stretching, particle-tracking microrheology, and so on, to better focus on AFM. As already anticipated, cell stiffness is assessed by means of force-distance curves, which should be properly fitted with contact mechanics models. Usually, the fitting is performed on the approach segment, in order to minimise the possible artifacts deriving from the adhesion between tip and sample.

Among the most common models used so far is Hertz model, which describes the contact of an elastic sphere pushed towards a rigid, flat substrate [45]. This theory is unfortunately limited to spherical indenters, but Sneddon extensions of the Hertz model take into account different indenter geometries. Other models like DMT (Derjagin, Muller, Toropov) and JKR (Johnson, Kendal, Roberts) are seldom used. In this thesis, we decided to align with the majority of existing works and apply Hertz model and its extensions, depending on the tip shape. Despite this choice could rise controversy, we pursued this approach because we did not intend to estimate absolute values, but perform comparisons among different conditions.

Hertz-Sneddon models for spherical and pyramidal indenters are reported in Figure 3.

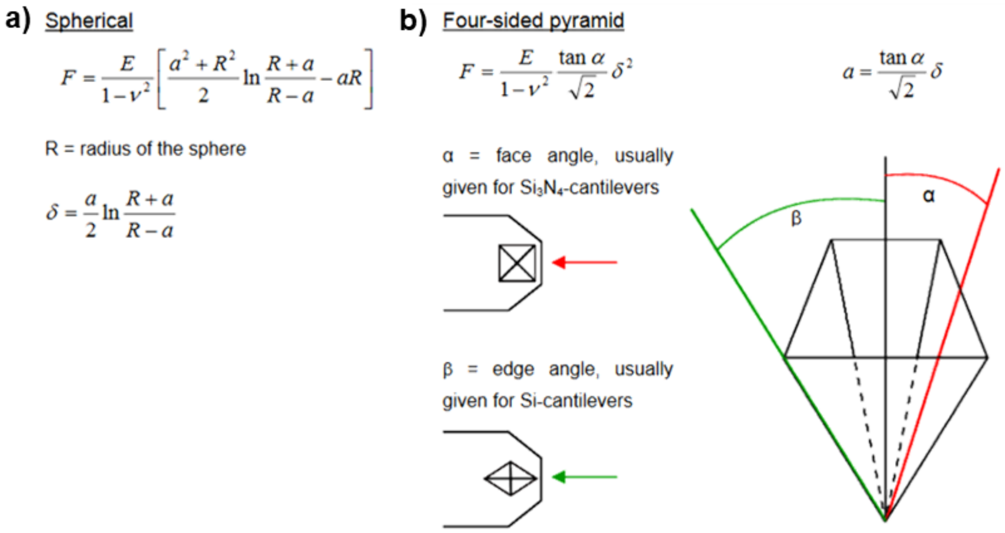
a) Spherical
$F = \frac{E}{1-\nu^2}\left[\frac{a^2+R^2}{2}\ln\frac{R+a}{R-a} - aR\right]$
R = radius of the sphere
$\delta = \frac{a}{2}\ln\frac{R+a}{R-a}$
b) Four-sided pyramid
$F = \frac{E}{1-\nu^2}\frac{\tan\alpha}{\sqrt{2}}\delta^2$
$a = \frac{\tan\alpha}{\sqrt{2}}\delta$
α = face angle, usually given for Si₃N₄-cantilevers
β = edge angle, usually given for Si-cantilevers
α
β

Figure 3 *Hertz-Sneddon models for spheres (a) and four-sided pyramids (b). F is the force, δ the indentation, E the Young's modulus, and ν the Poisson's ratio. This picture is extracted from reference* [46].

We will now give an overview on the literature about the assessment of cell stiffness by atomic force microscopy.

Cell stiffness has played a key role in the study of cancer, which is the most common disease studied by means of AFM so far. Already in 1999, Malgorzata Lekka and her group were exploiting AFM to study normal and cancerous human bladder cells. Authors showed that cancerous cells were softer and easier to deform respect to controls [47]. This groundbreaking work put the spotlight on the use of AFM for studying cancer and paved the way for the plethora of papers that followed. For instance, in 2007, Cross and colleagues measured the stiffness of benign and metastatic cells derived from pleural effusions of patients with suspected metastatic adenocarcinoma, finding out again that metastatic cells were overall softer than benign counterpart [48]. Over the years, a wide spectrum of tumors has been investigated, covering various cancerous sites (like breast in [49] and ovaries in [50]) and stages (such as in [51]). Cancer cell stiffness under the effect of certain events has been also measured by AFM. For example, the proximity of other cells was shown to influence the stiffness of normal mammary epithelial cells, which were softer if located at the periphery of a contiguous cell monolayer [52]. Moreover, cancer cells were found to be less sensitive to the presence of neighbouring cells than controls [52]. AFM proved to be useful even in the study of the effects that transforming growth factor-β (TGF-β), a cytokine upregulated in breast cancer, has on tumor cells with different invasiveness [53]. Looking at potential rescue mechanisms, the administration of green tea extract, a substance known as a potential anticancer agent, was proven effective, since raised the stiffness of metastatic tumor cells to normal values [54]. Given the fact that most of chemotherapeutic agents damage cardiac cells, Yue et al. used AFM to bridge oncology and cardiology frameworks. Authors dosed primary cardiomyocytes from adult mice with doxorubicin (a well-known anticancer drug with cardiotoxic effects) and dexrazoxane (a cardioprotective agent), following different administration protocols [55]. Measuring cell stiffness revealed that cardiomyocytes benefit from the preadministration of dexrazoxane [55].

The promising results in cancer field led part of the scientific community to speculate the use of AFM as a routine technique for tumor diagnosis (see Figure 4). Nevertheless, it must be clear to the reader that many issues have to be tackled before AFM can become a routine technique in laboratory medicine.

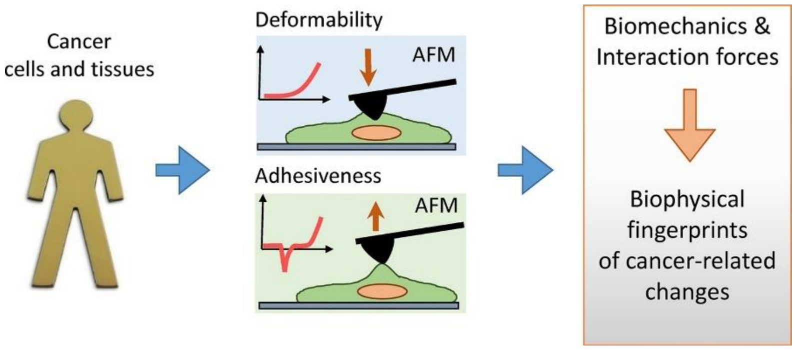
Cancer
cells and tissues
Deformability
AFM
Adhesiveness
AFM
Biomechanics & Interaction forces
Biophysical fingerprints of cancer-related changes

Figure 4 *Proposal for using AFM as a routine technique for cancer diagnosis (modified version from [56]).*

Besides cancer, AFM proved to be very sensitive in discerning other pathologic statuses. Back in 2005, Malgorzata Lekka and her group compared the deformability of erythrocytes from donors and hospitalised patients, who were suffering from several disorders (coronary disease, hypertension, diabetes mellitus) [57]. Authors highlighted an increase in the Young's modulus of erythrocytes derived from diabetes mellitus patients, as well as from cigarette smokers [58]. Pathological erythrocytes were shown to be stiffer than healthy ones even in the context of anemias and anysocytosis [59].

The consequences of diabetes were observed also in cardiomyocytes from a murine model, finding out that the disease caused an increase of stiffness of the myocardium [60].

Since the scope of our thesis is to show the power of AFM in the study of genetic diseases, it is worth mentioning that the technique was already exploited in this sense, but few papers are so far available. In this regard, studies on progeria *in vitro* models were remarkable, but they will described in the dedicated section. DCM was previously investigated by our group, but mutations in *LMNA* were considered. Indeed, Laurini et al. studied three *LMNA* mutations (E161K, D192G, N195K) known to cause DCM, discovering that these produce an increase of the Young's modulus of neonatal rat cardiac myocytes [61]. A genetic cardiocutaneous disorder associated with a desmoplakin mutation has also been recently studied by our group with AFM, and keratinocytes derived from a patient skin biopsy exhibited a higher deformability (lower stiffness) than controls [62].

1.5.1 Who contributes to cell stiffness?

In eukaryotic cells, the major contributors to the overall stiffness are cytoskeleton and nucleus.

This section, except if otherwise specified, is referred to the works of Fletcher and Mullins [63] and Lammerding [64].

1.5.1.1 The cytoskeleton

Cytoskeleton is the network that spatially organises the cytoplasm, connects the cell to the external environment, and develops forces that allow the cell to change its shape and move. It is mainly composed by microfilaments, microtubules, and intermediate filaments (IFs), which are all interconnected to each other, forming an intricate system. The interactions between the various elements can be either specific or non-specific. The former are the ones involving other kind of proteins, while the latter are steric interactions and entanglement.

Cytoskeletal components are primarily discerned by their mechanical stiffness, the dynamics of their assembly, their polarity, and the molecular motors to which they associate.

Microfilaments, frequently called actin filaments, are polymers made of smaller, globular, and compact subunits of actin. The smaller subunits can diffuse fast within the cytoplasm, whilst filamentous assemblies cannot [65]. Cells can therefore reorganise their structure rapidly, depending on their needs and/or the stimuli they sense [65]. Actin filaments, as well as microtubules, are polarised polymers, since their subunits are asymmetrical at the molecular level. Because of their polarity, actin filaments and microtubules are appropriate tracks for the molecular motors that has one preferential direction of movement. The molecular motors for microfilaments belong mainly to the myosin family, whereas for microtubules are from dynein or kinesin families.

The most complex dynamics for assembly and disassembly is that of microtubules, which are also the stiffest among the cytoskeletal components.

The constitutive subunit of microtubules is tubulin [65], and these subunits polymerise to form polarised structures.

Intermediate filaments are not polarised, so they are not suitable for molecular motors with a directional movement. These filaments are the least stiff and can resist tensile forces better than compressive loads. The constitutive subunit of IFs is a monomer with a central α-helical core, preceded by a globular N-terminal domain, and followed by a C-terminal domain. When two monomers associate, a coiled-coil dimer is formed; when two dimers with antiparallel orientation pair, a tetramer is generated. Finally, tetramers assembly to produce more complex structures, as shown in Figure 5.

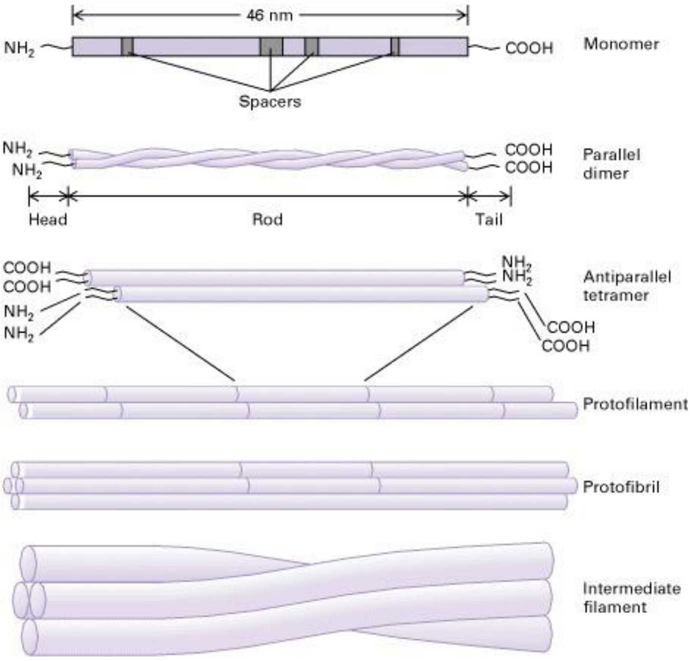
46 nm
NH2
COOH
Monomer
Spacers
NH2
NH2
COOH
COOH
Parallel dimer
Head
Rod
Tail
COOH
COOH
NH2
NH2
NH2
NH2
Antiparallel tetramer
COOH
COOH
Protofilament
Protofibril
Intermediate filament

Figure 5 *Assembly of intermediate filaments (from [66]).*

1.5.1.2 The nucleus

The nucleus is a unique characteristic of eukaryotes, and is the largest organelle in most cells. Usually, cells contain one nucleus, except cardiomyocytes and skeletal muscle cells that are polinucleated, and mature erythrocytes that no longer have it.

Nucleus and its content are separated from the cytoplasm by the nuclear envelope (NE), which is composed by two nuclear membranes (the inner and the outer), the nuclear lamina, and the nuclear pore complexes (NPCs) [67]. Nuclear membranes are phospholipid bilayers, and provide a physical separation between content of the nucleus and cytoplasm. Nuclear membranes are linked by NPCs, which act as channels for the selective traffic of proteins and RNAs between cytoplasm and nucleus [67]. The nuclear lamina is a dense, fibrous meshwork made of lamins and lamin-associated proteins (LAPs), and lies underneath the inner nuclear membrane. It plays a leading role in providing strength and integrity to the nucleus.

Inside the nucleus are chromatin, nucleoskeleton, and other structures like the nucleolus. Chromatin is mainly classified in euchromatin and heterochromatin, depending on their ability to be transcripted or not. The nucleskeleton is primarily composed by lamins, but short actin structures were also observed. Nucleskeleton is connected with cytoskeleton through the LINC (linker of nucleoskeleton ad cytoskeleton) complex, which is predominantly formed by nesprins and SUN proteins. Last, the nucleolus is the site where the ribosomal subunits are assembled.

The impetus for studying the structural and mechanical properties of nuclei was given by the observation that defective nuclear mechanics was associated with impaired cellular functions and the onset of pathologic conditions.

Over the years, it has been shown that nuclear stiffness is crucial, and the nucleus may be 5 to 10 times stiffer than the cytoskeleton in differentiated cells. Among the nuclear components, most of the structural and mechanical properties is provided by the nuclear lamina, which acts as an elastic, load-bearing element, in particular under the application of a tensile load. Conversely, the nuclear interior behaves as a viscoelastic solid, thus can be modelled by a spring (elastic contribute) and a dashpot (viscous contribute) [68]. This behaviour is typical for most entangled semi-flexible polymers, hence the viscoelastic nature is most likely caused by entangled DNA structures [68]. Chromatin is thought to play a main role in nuclear stiffness, since its stiffening was detected after alteration with divalent salts or upregulation of heterochromatin proteins. The contribute of short actin structures is still unknown, but probably they do not provide the same strength that has been observed in cytoskeleton [68]. Finally, inner and outer membranes have a marginal influence on nuclear stiffness, because they behave as 2-dimensional fluids.

1.6 Measuring the adhesion by AFM

Cell adhesion is the process by which a cell binds to another entity, such as another cell, a substrate, or an organic matrix.

Before getting further into this section, we must ask ourselves a question, as we did for cell stiffness: "**why should we investigate the adhesiveness of a cell, and how**?".

The answer lies in the fact that cell adhesion is fundamental in many processes, like cell communication, tissue development and maintenance. Cell adhesion acts as a trigger for signals regulating cell differentiation, cell cycle, migration, and survival [69], and the interactions between cells and extracellular matrix (ECM) can influence cell behaviour and functions. Furthermore, cell adhesion plays a key role in health and disease: for example, abnormal adhesion mechanisms have been discovered in correlation with the progression of cancer [70]. Last but not least, the impairment of adhesiveness is typical in the pathogenesis of certain diseases, like AC, where the speculated detachment of cardiomyocytes due to altered cell-cell junctions is thought to trigger the disorder.

As well as cell stiffness, numerous techniques have been used for measuring cell adhesion, such as micropipette aspiration, wash and centrifugation assays, traction force assays, quartz crystal microbalance techniques, and so on. However, this thesis is about AFM, so we will focus on this.

Adhesive properties and events are usually derived from the retraction segment of a F-d curve. The overall cell adhesion may be described by the maximum adhesion force, the distance at which this force occurs, and the work of adhesion (see Figure 6).

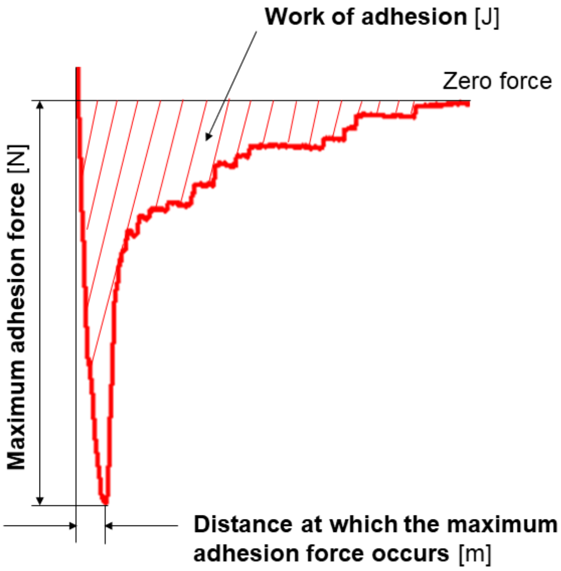
Work of adhesion [J]
Zero force
Maximum adhesion force [N]
Distance at which the maximum adhesion force occurs [m]

Figure 6 *Adhesive properties that can be extracted from the retraction segment of F-d curves.*

The maximum adhesion force, also called maximum detachment force, is represented by the peak of force respect to the zero force value. The distance at which this force occurs is calculated from the beginning of the withdrawal until the appearance of the peak. Finally, the work of adhesion, known as work of detachment, defines the energy dissipated during the retraction of the probe from the sample, and is calculated by integrating the area above the retract F-d curve and the zero force value.

“Single” bonds can be also inferred from F-d curves, looking at ruptures and tethers. The former are referred to cell adhesion receptors which are anchored to the cytoskeleton, whereas the latter involve receptors not linked to the cytoskeleton [10].

For the sake of completeness, it is worth noting that there are two main configurations to measure cell adhesion [10] [Friedrichs et al., 2013]:

I. a cell on a substrate is "touched" by either a tipless cantilever or a cantilever-tip assembly;
II. a cell adhered to the cantilever is brought in contact with either a substrate or another cell.

In both cases, the substrate or the cantilever can be functionalised with proteins of interest (e.g. ECM proteins). In both configurations, specific adhesive bonds can be assessed, if the cantilver has been previously functionalised or one cell is probed on top of another one; otherwise, nonspecific interactions are measured. In this thesis, since we want to perform preliminary studies that can show the power of the AFM in assessing the behaviour of cells with genetic mutations, we decided to measure nonspecific cell adhesion. Further experiments to investigate specific adhesive properties may be planned after the evaluation of preliminary data here presented.

Following the same outline of section 1.5, the reader will now get in contact with some works about cell adhesion assessed by means of AFM.

In 1998, Thie et al. aimed to unravel the mechanisms behind embryo implantation, thus they investigated the interactions between a human trophoblast-type cell (JAR) and two types of human uterine epithelial cell line (RL95-2 and HEC-1-A), finding out that the bond "JAR-RL95-2" is stronger than the one formed by JAR and HEC-1-A [71]. Benoit and Gaub exploited the second configuration earlier mentioned to show the versatility of AFM in the study of cell adhesion: they probed bone cells (SaOS2) towards different substrates, and red blood cells against each other [72]. Notably, they discovered that erythrocytes have null adhesion in PBS, whereas lectin addition triggered an adhesive phenomenon between the cells [72]. Configuration II was then used to probe zebrafish primary mesendodermal progenitors against fibronectin-coated substrates. First, cells derived from wild type and *slb/wnt11* mutant models were captured by a concanavalin A-functionalised cantilever [73]. Experiments demonstrated that mutant cells can "stick" less to fibronectin than wild type, and this was due to the loss-of-function mutation in Wnt11 [73]. Again, cell-cell and cell-substrate interactions were studied lowering a WM115 cell (melanoma cell line) on either a fibronectin-coated substrate or a HUVEC cells layer [74]. Interestingly, the small adhesion events observed in the curves among WM115 cell and fibronectin disappeared after administration of RGD peptide because it competed with fibronectin to bind integrins [74]. Moreover, AFM detected a decrease in the number of the small events also in the curves between WM115 and HUVEC after calcium removal [74].

Sarah E. Cross and her group analysed cells from pleural effusions to find differences in the adhesive properties of normal and tumor cells. Nonspecific cell adhesion of tumor cells was found to be lower than that of normal cells, although measuring the specific interactions was strongly recommended before choosing adhesive properties as a marker for cancer cells evaluation [75]. As well as Cross and coworkers, Laurini et al. studied nonspecific interactions, and observed that three *LMNA* mutations causing DCM induced a decrease of the work of adhesion in neonatal rat cardiomyocytes, compared to controls [61].

1.6.1 Who contributes to cell adhesion?

Cell adhesion is mediated by cell adhesion molecules (CAMs), a set of proteins located on the cell surface that bind one cell to other cells or its surroundings. CAMs are usually divided in five classes: integrins, selectins, cadherins, immunoglobulin superfamily, and CD44 family [76].

When a binding occurs, the resulting structures are called cell junctions. The main cell junctions are: hemidesmosomes, focal adhesions, adherens junctions, tight junctions, gap junctions, chemical synapses, and desmosomes [77]. Hemidesmosomes and focal adhesions refer to the link between a cell and the surrounding environment (e.g. extracellular matrix), whereas the others involve neighbouring cells. We will now give a glimpse of the different cell junctions, apart from chemical synapses, since these are exclusive to nerve cells and therefore outside of the scope of this work. As one of the genes studied in the thesis affects desmosomes, we will dedicate a distinct section to these structures.

Hemidesmosomes and focal adhesions are mediated by integrins, and they serve as connection sites for intermediate filaments and microfilaments, respectively [77]. Adherens junctions connect the actin filaments of two adjacent cells, ataking advantage of cadherins [77]. Tight junctions, as indicated by the name, seal together the neighbouring cells to create a barrier impermeable to macromolecules [77]. Finally, gap junctions are usually described as narrow pores between adjacent cells, that are formed by clusters of channels [77].

1.6.1.1 Desmosomes

In 19th century, the Italian pathologist Giulio Bizzozero first observed certain small, dense nodes in the spinous layer of epidermis [78], but he was not aware that he was discovering one of the most crucial components in tissues exposed to mechanical stress. After being initially identified as “nodes of Bizzozero”, these complexes were later termed “desmosomes”, from the union of two Greek words, “desmo” and “soma”, meaning bond and body, respectively [78]. The desmosomal structure is depicted in Figure 7.

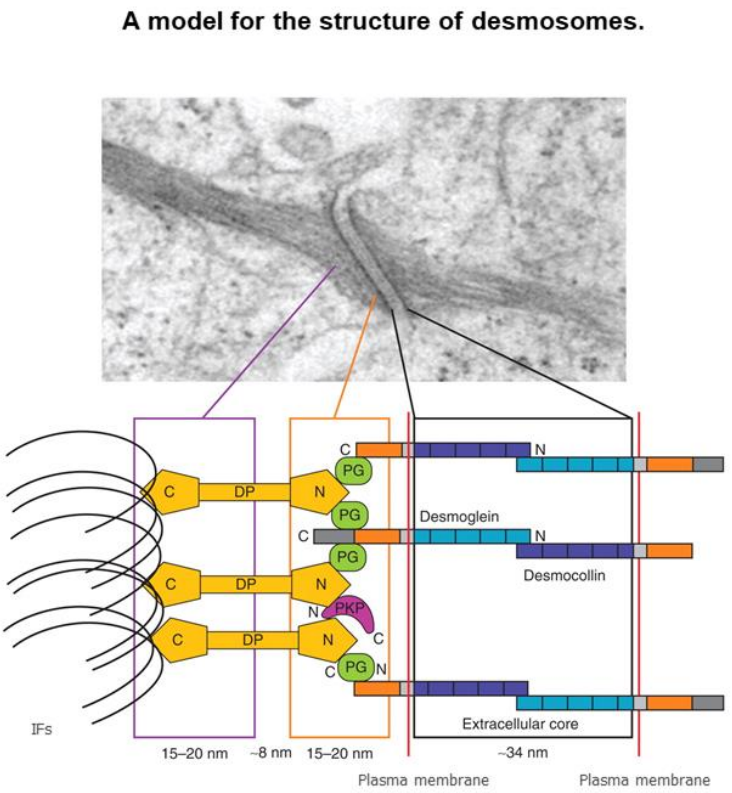

Figure 7 *Sketch of the desmosomal structure (adapted from* [78]*).*

Desmosomes tether intermediate filaments to the cell membrane, where they ended with proteins belonging to the cadherin family. The cytoplasmic part of desmosomes is formed by armadillo and plakin family members [79].

There are two types of desmosomal cadherins: desmocollins (Dscs) and desmogleins (Dsgs): three isoforms of Dscs and four of Dsgs are expressed in humans [78]. These cadherins are similar to classical cadherins because they have a series of highly conserved extracellular domains and a short transmembrane domain [79]. Although, classical cadherins bind to partners sharing their nature (homophilic manner), whilst Dscs and Dsgs interactions are still poorly understood [79]. The cytoplasmic side of desmosomal cadherins is linked to plakoglobin (Pg) and plakophilins (Pkps). Pg, also known as γ-catenin, contains 12 armadillo repeats, flanked by distinct N- and C-termini [78]; in humans, Pg is encoded by *JUP* gene. The central arm-domain of Pg interacts with desmoplakin (Dp), which in turn directly binds IFs [78]. Plakophilins will be described in detail in the chapter about AC.

Plakin family comprises desmoplakin, plectin, envoplakin, and periplakin [78]. Among them, Dp is essential for desmosome assembly and/or stabilization, and IFs anchorage: indeed, after ablation of the desmoplakin gene, murine embryos did not survive beyond E6.5 [80]. In humans, desmoplakin is encoded by *DSP* gene.

Based on the cell type, the intermediate filaments involved in the desmosomal junctions are distinct: for instance, keratins are present in most epithelial cells, whereas desmin is found in the myocardium [81].

Structurally, desmosomes are fundamental in tissues experiencing mechanical stress, like skin, bladder, gastrointestinal mucosa, and myocardium, which is the muscle that works the most in the body, contracting around 3 billion times in the life of a human [78]. Desmosomes are responsible for maintaining tissue integrity and providing tensile strength [82]. Desmosomes are peculiar junctions since they can exhibit two different adhesive states: one is calcium-dependent, whereas the other is a calcium-independent form. In the first state, desmosomes may lose adhesion and split in half, but the second is strongly adhesive and therefore is defined as "hyperadhesion" [83]. It has been speculated that hyperadhesion is a "normal" state, necessary to maintain tissue integrity; conversely, the calcium-dependent state is a "default" state that occurs when a weaker adhesion is required (e.g. in wound healing) [83].

Chapter 2: The genetic diseases

2.1 Arrhythmogenic cardiomyopathy

AC was first described by the Italian physician Giovanni Maria Lancisi in 1736 in his book *"De Motu Cordis et Aneurysmatibus"*. He reported the case of a family that, in four generations, showed palpitations, heart failure, dilation, aneurysms of the right ventricle and sudden death [84]. However, the first, large clinical study with 24 adult cases of "right ventricular dysplasia" dates back in 1982 [85].

The original designation of the disease was "arrhythmogenic right ventricular dysplasia" because it was considered an embryological aberration. Later, in order to take into account the fact that it was a genetically determined heart muscle disorder, the disease was termed "arrhythmogenic right ventricular cardiomyopathy" [86]. Over the years, many have reported cases that were slightly different from the original phenotype: the left ventricle involvement was indeed identical (biventricular AC) or greater (left-dominant AC) than the right ventricle involvement [86]. This has led to the diffusion of a broader definition, "arrhythmogenic cardiomyopathy", which attempts to cover all the phenotypes so far described [86]. In the present work, we align with the latest "trends", so we use the name "arrhythmogenic cardiomyopathy".

The disease usually starts from the right ventricle, where cell junctions fail to couple: defective cell-cell adhesion causes cardiac cells to "detach", inducing progressive loss of myocardium and subsequent fibrous or fibro-fatty replacement [87,88].

Classical symptoms such as palpitations and syncope are due to arrhythmias, but the first manifestation can be sudden death (SD) [89]. The clinical presentation is even more complex: clinical manifestations of this cardiomyopathy are highly variable [89].

AC onset and progression can be divided in three phases: concealed, overt, and cardiac failure [90]. In its early stages, AC is "silent", and patients are usually not aware of the disease. In this phase, SD may occur, especially after a strenuous effort (as during/after sport competitions). Notably, sport activities have been shown to worsen AC progression and increase the risk of SD in young and athletes [88]. In the second phase of the disease, patients exhibit overt symptoms with electrical and structural abnormalities evident during investigation. If the left ventricle is spared, AC patients can still cope with physical exercise, but SD is always a tangible threaten [90]. As the disease progresses, heart failure symptoms also develop.

AC cases may be infrequently diagnosed [91]. In 1994, an International Task Force identified major and minor criteria for AC diagnosis, based on a scoring system [92]. According to this Task Force, patients would have been diagnosed for AC if, and only if, the simultaneous presence of certain number and type (major/minor) of criteria was verified. The criteria are reported in Figure 8.

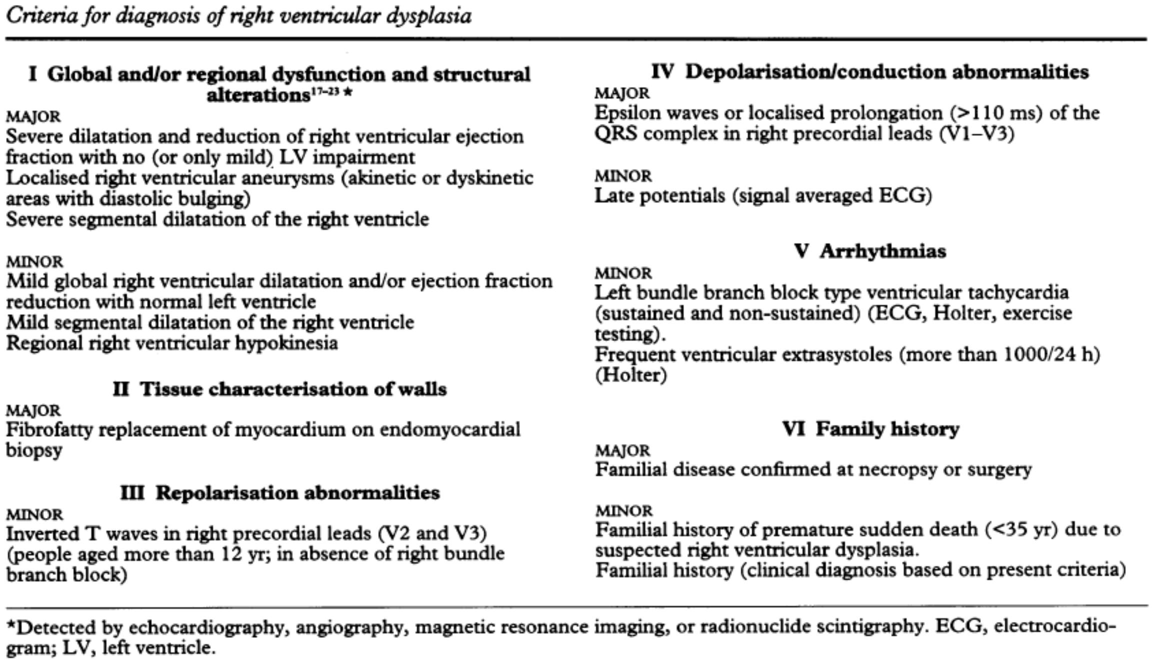

Criteria for diagnosis of right ventricular dysplasia

I Global and/or regional dysfunction and structural alterations[17–23] *

MAJOR
Severe dilatation and reduction of right ventricular ejection fraction with no (or only mild) LV impairment
Localised right ventricular aneurysms (akinetic or dyskinetic areas with diastolic bulging)
Severe segmental dilatation of the right ventricle

MINOR
Mild global right ventricular dilatation and/or ejection fraction reduction with normal left ventricle
Mild segmental dilatation of the right ventricle
Regional right ventricular hypokinesia

II Tissue characterisation of walls

MAJOR
Fibrofatty replacement of myocardium on endomyocardial biopsy

III Repolarisation abnormalities

MINOR
Inverted T waves in right precordial leads (V2 and V3) (people aged more than 12 yr; in absence of right bundle branch block)

IV Depolarisation/conduction abnormalities

MAJOR
Epsilon waves or localised prolongation (>110 ms) of the QRS complex in right precordial leads (V1–V3)

MINOR
Late potentials (signal averaged ECG)

V Arrhythmias

MINOR
Left bundle branch block type ventricular tachycardia (sustained and non-sustained) (ECG, Holter, exercise testing).
Frequent ventricular extrasystoles (more than 1000/24 h) (Holter)

VI Family history

MAJOR
Familial disease confirmed at necropsy or surgery

MINOR
Familial history of premature sudden death (<35 yr) due to suspected right ventricular dysplasia.
Familial history (clinical diagnosis based on present criteria)

*Detected by echocardiography, angiography, magnetic resonance imaging, or radionuclide scintigraphy. ECG, electrocardiogram; LV, left ventricle.

Figure 8 *Criteria for the diagnosis of AC established by an International Task Force in 1994 (adapted from [92]).*

In 2010, the criteria were updated in order to include novel diagnostic approaches/platforms and the newest discoveries about the genetic background of AC [93]. The additions increased the sensitivity of the diagnostic process, without affecting the specificity.

AC is usually diagnosed between 20 and 40 years of age, whilst diagnosis in pediatric age (0-18 years) is uncommon [94]. Indeed, AC morphofunctional phenotype is age-dependent, hence negative results are frequent in children and the young [95]. Children with potential to develop AC due to familial and/or personal history must be monitored carefully to identify the onset of the pathologic phenotype [95].

Treatment options include pharmacologic and nonpharmacologic therapies; among the latter are catheter ablation, implantable defibrillator (ICD), and, as final choice, heart transplantation [88]. According to the latest trends, gene therapies are being explored for AC, as proposed by researchers at UC San Diego [96].

AC is an inherited disorder, mostly transmitted with an autosomal dominant trait. Nonetheless, autosomal recessive forms have also been identified, i.e. Naxos disease and Carvajal syndrome. Naxos disease was first reported in the Aegean island of Naxos, whereas Carvajal - a variant of Naxos with more pronounced left ventricle involvement – was found in India and Ecuador [97]. In these two diseases, cardiac disorder is only one feature of the overall phenotype, which also comprises palmoplantar keratoderma and woolly hair [97].

2.1.1 Genetic background of AC

Nowadays, it is well-known that AC is an inherited heart muscle disorder; back in early 2000s, the evidence for the genetic etiology were still lacking. In their review dated 2001, Thiene and Basso reported certain potential causes for AC - besides genetic mutations -, including the involvement of viruses and an immune pathogenesis mechanism [90]. So far, several disease genes have been related to the onset of AC phenotypes (Table 1).

Gene	**Encoded protein**
PKP2	Plakophilin 2
DSP	Desmoplakin
DSG2	Desmoglein 2
DSC2	Desmocollin 2
JUP	Plakoglobin
CTNNA3	Alpha T-catenin
CDH2	N-cadherin
TMEM43	Transmembrane protein 43
TTN	Titin
FLNC	Filamin C
LMNA	Lamin A/C
TGFβ3	Transforming growth factor β3
PLN	Phospholamban
DES	Desmin
SCN5A	Voltage-gated sodium channel subunit alpha Nav1.5
TP63	Tumor protein p63
TJP1	Tight junction protein 1

Table 1 *Causal genes for AC known so far [98–100].*

AC-associated genes can be classified in two main groups: genes encoding desmosomal and non-desmosomal proteins, respectively.

2.1.1.1 Genes coding for desmosomal proteins

Mutations in genes coding for desmosomal protein account for almost half of the AC cases [101]. The mutations responsible for AC affect plakophilin-2 (PKP2), DSP, desmoglein-2 (DSG2), desmocollin-2 (DSC2), and PG (JUP). Section 2.1.2 will be entirely dedicated to *PKP2*, since it is one of the targets in this work.
The impetus for studying desmosomal proteins was the observation that in Naxos syndrome there is a deletion mutation in JUP [102]; in the following years, the other desmosomal genes were linked to AC [103–106]. Desmosomal mutations are responsible for both autosomal dominant and recessive forms of AC.

2.1.1.2 Genes coding for nondesmosomal proteins

Before going further, the reader must be aware that most of the non-desmosomal genes have been shown in AC patients only in isolated cases; lately, these clinical manifestations are being considered as phenocopies or overlap syndromes because the phenotype is similar, but not identical to AC [95]. Since the analysis of the whole spectrum of genes inducing AC phenotype is outside the aim of the work, this section will focus only on two genes reported in Figure 8, among the non-desmosomal ones, which have proven familial basis.
The first gene is *TMEM43*, which encodes for TMEM43, also known as LUMA, namely a putative membrane protein of which very little is known [107]. In 2008, families from Newfoundland island with AC type 5 were shown to carry a mutation (p.S358L) in *TMEM43* [108]. Within this thesis, it is worth to mention that dermal fibroblasts of p.S358L mutation carriers were probed by AFM. Nuclei of mutant cells were proven to be stiffer than wild-type counterpart, thus paving the way of AFM into AC field [109].
The second gene we will investigate is *LMNA*. Recently, Lamin A/C has raised a great interest in the scientific community because mutations in *LMNA* are responsible for a broad spectrum of pathologies, collectively known as laminopathies. These diseases share *LMNA* mutations as common cause, but range from tissue-specific disorders (e.g. AC-like phenotypes) to systemic conditions (e.g. progeria). In 2012, *LMNA* mutations were identified in severe forms of AC, and the addition of *LMNA* in the genetic screening for patients with suspected AC was suggested [110]. Later on, two other AC patients with *LMNA* mutations were found in a Japanese cohort [111]. As earlier anticipated, LMNA-AC phenotype is being recently considered an overlap syndrome, because the pathogenic phenotype cannot be considered identical to AC [95].

2.1.2 PKP2 at a glance

Plakophilin 2 is part of the plakophilins family, together with plakophilin 1 and 3. As stated in paragraph 1.6.1.1, plakophilins belong to the larger class of Armadillo proteins, which are characterised by a repeating 42 amino acid motif, made of α-helices [112]. The series of 10 imperfect armadillo repeats is preceded by an amino-terminal head and followed by a short carboxyl-terminal tail [113,114]. PKP2, as well as plakophilin 1, has two isoforms: one is shorter ("a" form), while the other is longer ("b" form) [79].

In humans, PKP2 is encoded by *PKP2* gene. In cells forming desmosomes, plakophilins have been found in both desmosomes and nuclei, whereas in cells without desmosome, plakophilins have been detected only in the nucleus [114]. Plakophilins are responsible for the connection of desmosomal cadherins with desmoplakin and the intermediate filaments.

Being part of the desmosome, plakophilin 2 is heavily involved in cell-cell adhesion, cell signaling, tissue morphogenesis, and differentiation [115]. A detailed review of PKP2 functions is provided in the work of Neuber and co-authors [116].

The potential link between *PKP2* mutations and AC was first speculated by Gerull and coworkers in 2004 [104]. Nonetheless, as reported by Syrris et al. two years later, this study was lacking in detailed clinical evaluation of the probands and data on family members [115]. Therefore, the first, demonstrated link *PKP2*-AC must be considered the one proposed by Syrris and colleagues, who found 9 PKP2 variants in 11 cases of familial AC, without cutaneous manifestations [115]. Since 2006, increasing evidence has led to the discovery that *PKP2* is the most common disease gene in AC, with an estimated prevalence from 7 to 51%, and spikes reaching 70% [117].

Interestingly, *PKP2* mutations have been associated with Brugada syndrome (BS), an electrical heart disorder. 30% of BS patients carry *SCN5A* mutations, and *SCN5A* codes for sodium channels. Lately, Brugada syndrome and AC are considered to be sharing a common origin, so they could not be two different pathologic entities [118]. This idea has been strengthened by the fact that *PKP2* variants may be found in BS cohort, and then can be implicated in the onset of the disease [119].

PKP2 has been also proposed as a marker for cardiac myxomata, a kind of benign tumor characterised by connective tissue embedded in mucus and most likely derived from cardiac mesenchymal cells [120]. Indeed, all adherens junctions between cells of cardiac myxomata showed the presence of PKP2, as observed by Rickelt et al. in 2010 [120].

To the best of our knowledge, AFM has been applied to PKP2 mutant cells only by our research group (manuscript submitted for publication).

2.2 Dilated cardiomyopathy

DCM is a genetically determined heart muscle disorder and the most common cardiomyopathy worldwide [121]. It is characterised by the enlargement of one or both ventricles and an impaired systolic function, in the absence of abnormal loading conditions (e.g. pressure/volume overload or coronary artery disease) that could otherwise explain the dysfunction [122,123].
DCM is diagnosed if two major criteria are fulfilled:

1) left ventricular fractional shortening less than 25% and/or LVEF less than 45%;
2) left ventricular end diastolic diameter greater than 117% of the predicted value corrected for age and body surface area per the Henry's formula [121].

Usually, DCM is diagnosed between 30 and 40 years of age, but is also one of the most common forms of cardiomyopathy in children [123,124]. Notably, recent evidence confirms that pediatric and adult dilated cardiomyopathies are "distinct pathological entities" [125]. For example, Tatman and colleagues observed unique changes in gene expression of pediatric DCM hearts, which were not found in adult samples [126]. Moreover, no adverse remodeling phenomenon was detected in children, whereas it was present in adults [125]. These indications may potentially help physicians in finding effective treatments for pediatric patients, since therapies for adults are often failing with children [125].
DCM can be treated with both pharmacologic and nonpharmacologic approaches. The first include for instance β-blockers, whereas the latter can be either ICD or transplantation.
According to literature, DCM onset can be triggered by genetic, infectious, autoimmune, and toxic causes [127]. In most cases (up to 50%), no definite cause is yet identified, and DCM is therefore defined as "idiopathic" [127,128]. Maron and coauthors described DCM etiology as "mixed", i.e. both genetic and nongenetic; notably, genetic DCM accounts for up to 40% of the set [123,127]. 20-35% of DCM cases have been identified as familial, therefore with two or more family members affected by the same disease [121][Sweet et al., 2015]. Nonetheless, familial DCM is recognised also if a first-degree relative of DCM patients unexpectedly dies from SD before the age of 35 years [129].
Familial DCM are mostly transmitted via an autosomal dominant trait, but autosomal recessive, X-linked and mitochondrial forms have been seldom reported [130].

2.2.1 Genetic background of DCM

In this section, we will look at two genes (*TTN* and *LMNA*) in the wide spectrum of DCM disease genes, which currently comprises over 40 genes [131]. If further details are required, DCM genetic background is thoroughly reviewed in the paper of McNally and Mestroni [132].

So far, DCM has been associated with mutations in genes involved in sarcomere, cytoskeleton, nuclear envelope, and sarcolemma structures, but also calcium cycling, RNA splicing, and protein trafficking [130].

Titin (TTN) is a giant protein (~ 1 μm long), encoded in humans by *TTN* gene, and expressed in striated and cardiac muscles [133]. It spans from the Z-disc to the M-line of the sarcomere, and plays a key role in the assembly and functioning of muscles [133]. Titin mutations were early associated with the onset of familial DCM, as shown in 2002 by Gerull and coauthors [134]. Nowadays, *TTN* is recognonised as the most common disease gene in DCM [135], in particular after the groundbreaking study of Herman et al., in which authors reported that around 30% of DCM patients carry a *TTN* mutation [136]. Interestingly, titin has been widely studied via AFM, exploiting a technique that allows to pull and stretch single molecules. A comprehensive review was published by Linke and Grützner [137].

LMNA has been already introduced in the AC section. Within the huge variety of diseases caused by *LMNA* mutations, there is also DCM. In 1994, Kass et al. described a gene defect at locus 1p1-1q1 that was associated with conduction system disease and DCM; however, the candidate genes were not identified [138]. Later on, Fatkin and coworkers further explored these data and were the first to report *LMNA* mutations as causes of DCM and conduction system disease [139]. DCM was confirmed then in *Lmna* $^{-/-}$ mice, which manifested dilated cardiomyopathy and conduction abnormalities by 4-6 weeks of age [140]. Further details about lamin A/C and DCM are reviewed in [141–143].

In the next paragraphs, we will have a closer look at *FLNC*, a gene that has been recently discovered in association with DCM and other forms of cardiomyopathy.

2.2.2 FLNC at a glance

Filamin C, also known as filamin 2, is one of the three isoforms of filamins expressed in mammals. As well as the other isoforms, FLNC is a dimer with a flexible V-shaped structure. Each monomer consists of three main regions: head, backbone, and tail [144]. The head of filamins is a N-terminal actin-binding domain; it is followed by the backbone, namely a rod region composed by 24 immunoglobulin-like repeats [144,145]. The 24th repeat is the tail region and identifies the self-association domain, that is where two filamin monomers can dimerise [144,146]. Figure 9 depicts the general structure pf filamins.

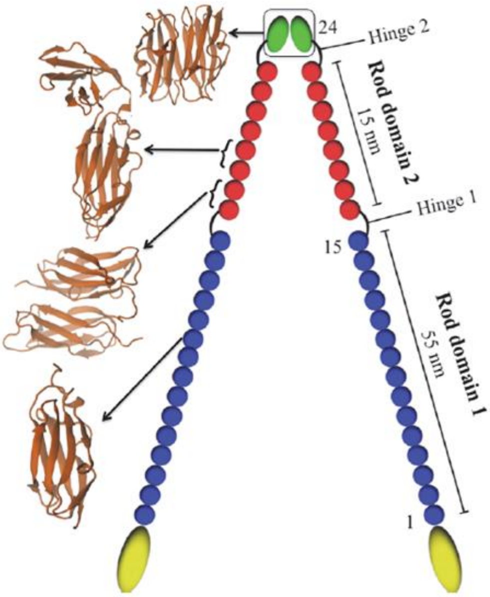

Figure 10 *Schematic structure of filamins (adapted from [144]).*

In humans, FLNC is encoded by *FLNC* gene, and in adults its expression is mostly restricted to cardiac and skeletal muscles [147]. Though the exact function of filamins is yet to be fully understood, it is well-established that filamins are actin-binding proteins. They were among the first actin-binding molecules to be discovered, certainly the first non-muscle actin binding proteins [147]. In 1978, Brotschi et al. showed that actin forms 3D networks in presence of so called actin gelling factors, like filamin [148]. The orthogonal networks of actin formed by filamins can be viewed in the paper of Stossel et al. [145].

Besides actin, filamins have been shown to interact with more than 90 different proteins, included but not limited to dystrophin-glycoprotein complex (DGC), integrin, myotilin, FATZ, and myopodin [146,149]. Because of this large number of interactions, filamins are thought to be involved in many processes, like cell-cell and cell-ECM adhesion, actin remodeling, mechanoprotection, and several signaling pathways [146]. Some of these interactions suggest FLNC to contribute to the mechanical stability of the sarcomere [150]. Therefore, if a mutation occurs, most likely there will be an impairment of the cell mechanical behaviour/mechanics.

FLNC mutations were first described in myopathies, then in heart muscle disorders. In 2014, variants in *FLNC* were identified in patients suffering from hypertrophic cardiomyopathy, who were showing marked abnormalities in the sarcomere of cardiac muscle [151]. One year later, Brodehl and colleagues reported *FLNC* mutations as cause of autosomal dominant restrictive cardiomyopathy [152]. The first association between *FLNC* and DCM was the observation of putative mutation in *FLNC* in a DCM patient, but the pathogenicity was not demonstrated [153]. The first pathogenic mutation was identified in 2016 by Begay et al.: families from Italy and US, affected by DCM, were *FLNC* mutations carriers [150]. Authors confirmed the pathogenicity of *FLNC* mutations knocking down the ortholog *flncb* in zebrafish, and observing the manifestation of a cardiac dysfunction phenotype [150]. Similarly, the *FLNC* variants found by Reinstein and co-authors caused a devastating DCM phenotype when co-expressed, alongside the deposition of filamin C aggregates [154]. Mutant filamin C proteins were observed also in a cohort of patients previously diagnosed for DCM, AC, and restrictive cardiomyopathy: truncating *FLNC* mutations were then associated with the onset of an overlap syndrome between DCM and AC [155].

After this promising evidence, finding a link between FLNC and cardiomyopathies has become a hot topic in the scientific community. Only in 2018, *FLNC* mutations have been found to cause adult-onset familial DCM in Iceland [156], and a cardiac-restricted arrhythmogenic DCM phenotype [157]. Future perspectives in the study of FLNC-associated cardiomyopathies have been recently highlighted by Corrado and Zorzi [158].

2.3 Hutchinson-Gilford progeria syndrome

Progeria is a rare, genetic disorder causing premature and accelerated ageing. The term progeria derives from two Greek words, “pro” and “gēras”, namely “before, premature” and “old age”.

Usually, children appear normal at birth, but within the first year, they start manifesting the typical features of the disease [159]. The syndrome is characterised by a wide spectrum of clinical features, including growth retardation, alopecia, prominent eyes ad scalp vasculature, lipodystrophy, micrognathia, and atherosclerosis; mental development is generally normal [160–162]. Often, HGPS patients die during puberty (averagely 13 years of age) because of cardiovascular complications [160,163].

The disease was first described in England by Hutchinson and Gilford, in 1886 and 1904 respectively [164]. Progeria affects 1 in 20 million people, with 350-400 HGPS children estimated to live at any one time [165].

HGPS is diagnosed based on the typical signs and symptoms described above (see Figure 10). Genetic tests are performed to confirm the diagnosis.

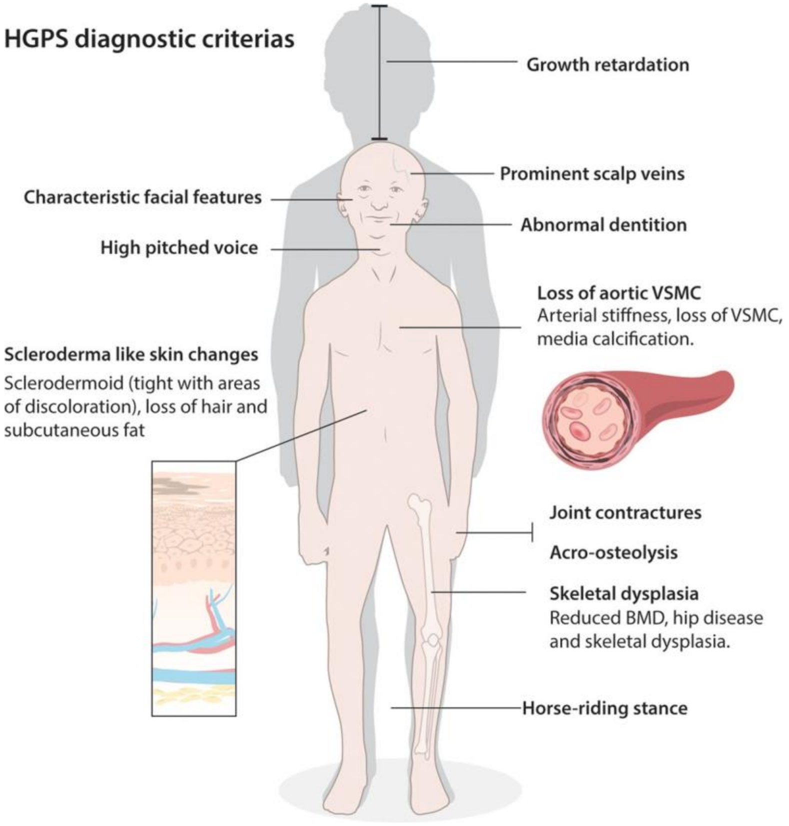
HGPS diagnostic criterias
Growth retardation
Prominent scalp veins
Characteristic facial features
Abnormal dentition
High pitched voice
Loss of aortic VSMC
Arterial stiffness, loss of VSMC, media calcification.
Scleroderma like skin changes
Sclerodermoid (tight with areas of discoloration), loss of hair and subcutaneous fat
Joint contractures
Acro-osteolysis
Skeletal dysplasia
Reduced BMD, hip disease and skeletal dysplasia.
Horse-riding stance

Figure 11 *Main diagnostic criteria for HGPS* [166].

To date, no treatment has been proven effective yet. Therapeutic approaches are usually targeted to alleviate the symptoms or prevent certain events (e.g. administration of low doses of aspirin to prevent thromboembolic episodes) [167]. Harhouri and coauthors have recently published a thorough review of treatment strategies [161].

HGPS is a laminopathy, in fact is caused by mutations in *LMNA*. Both autosomal dominant and recessive forms of progeria have been either reported or hypothesised so far. The most common trait is autosomal dominant, but recessive inheritance has been suggested in certain works, for example by Gabr et al., who described two affected sisters [168].

In the next section, the genetic background of progeria will be described, focusing on the alterations of *LMNA* and the consequent effects.

2.3.1 Genetic background of HGPS and LMNA at a glance

2003 was a turning point in the study of progeria: that year, two independent groups reported *LMNA* mutations as cause of HGPS. Before, HGPS gene was “localised” to chromosome 1q, but no disease gene was clearly identified [169]. De Sandre-Giovannoli and colleagues described two patients carrying a heterozygous C to T substitution at nucleotide 1824 in April 2003, whilst Eriksson and coauthors published their results on 23 cases of classical HGPS later in May 2003 [169,170]. In 18 patients, Eriksson and her group observed in the same silent single-base substitution (G608G) identified by De Sandre-Giovannoli et al.; they found also other mutations in two cases (G608S and E145K, respectively) [169]. The absence of G608G, G608S, and E145K mutations in parents allowed confirming the *de novo* nature of the mutation (*nota bene*: only 8 cases with G608G were considered) [169].

Up to now, 14 different mutations have been identified as causative of HGPS, but the most common mutation remains G608G [171,172].

In humans, the alternative splicing of *LMNA* produces lamin A, lamin C, and two minor isoforms (lamin AΔ10 and lamin C2, respectively) [173]. These are collectively known as A-type lamins, and are type V intermediate filaments. As well as other IFs, A-type lamins have a short N-terminal head, followed by a α-helical central rod domain, and end in a carboxyl-terminus that comprises also an immunoglobulin-like domain [173,174].

Lamin A and lamin C are identical, except for the C-terminus, where lamin A has 98 amminoacids (AAs) more than lamin C (Figure 11) [175]. In lamin A, the AAs form a CAAX motif, which is crucial for the posttranslational modifications leading to the insertion of lamin A in the nuclear lamina [175].

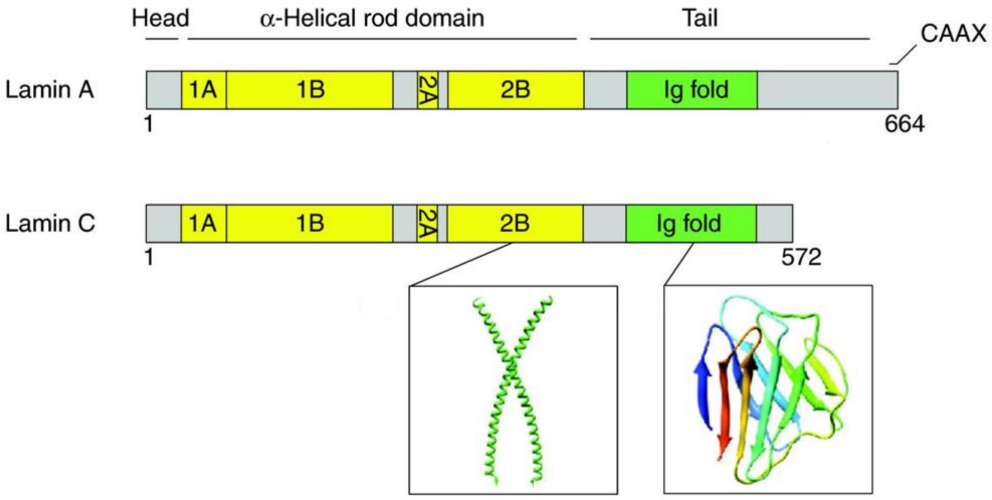

Figure 12 *Lamin structure and domain organisation (modified version of [176]).*

Lamin A is produced as a precursor, called prelamin A, that undergoes several processes. The complete maturation of lamin A lasts around 3 hours, and is depicted in Figure 12 [177]. In HGPS, the genetic mutations cause an accumulation of a truncated form of prelamin A, known as progerin [178].

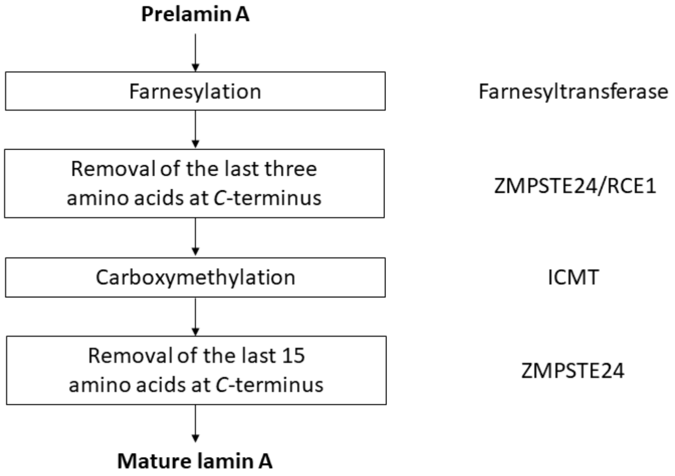
Prelamin A
Farnesylation
Farnesyltransferase
Removal of the last three amino acids at *C*-terminus
ZMPSTE24/RCE1
Carboxymethylation
ICMT
Removal of the last 15 amino acids at *C*-terminus
ZMPSTE24
Mature lamin A

Figure 13 *Posttranslational modifications of prelamin A (adapted from [177]).*

Though lamins are part of the nuclear lamina, they have been observed also in the nucleoplasm and in association with sites of DNA replication [174]. Over the years, many functions of lamins have been revealed, but the whole spectrum of their activities remains elusive. The reader may find an introductory perspective on the functions fulfilled by lamins in one of our papers [174]. Here, we will focus on the role played by lamin A/C in cell mechanics. The first evidence of this was provided by studies of *Xenopus* oocytes. Dahl et al. studied isolated *Xenopus* oocyte nuclei via micropipette aspiration, finding out that the nuclear lamina is extensible, but has a compressibility limit, and therefore acts as a molecular shock absorber [179]. The same model (isolated nuclei of amphibian oocytes) was later investigated by AFM, after ectopical expression of lamin A. Nuclear stiffness of mutants was higher than in controls, depending upon the level of lamin expressed (which in turn was based on the concentration of DNA injected) [180]. On the other hand, Kauffmann et al. injected amphibian oocytes to ectopically express either wild type or mutant (E145K) lamin A. Isolated nuclei were probed by AFM, revealing an increase of the stiffness due to the abnormal protein [181]. Nuclei isolation was crucial even in the work of Apte and colleagues, who studied dermal fibroblasts from a progeria patient. In the paper, skin fibroblasts were derived from one progeria patient, a young (10 years old) donor, and an old (61 years old) one [182]. Whilst no significant difference was detected among the groups in the overall, isolation of the nuclei showed a different mechanics (i.e. Young's modulus), and an increase in stiffness due to progeria and/or age [182]. Conversely, mouse embryonic fibroblasts (MEFs) with lamin A/C deficiency (MEF$^{-/-}$) exhibited reduced stiffness and lost their integrity after compression experiments, if compared to wild type samples (MEF$^{+/+}$) [183]. Same conclusions were achieved by Lammerding and his group with other techniques: lamin-deficient MEFs displayed both increased nuclear deformability and lower cytoskeletal stiffness [184].

Chapter 3: Materials and Methods

3.1 Cell culture

3.1.1 AC/*PKP2* framework

Mouse atrial cells, HL-1 (WT) and PKP2-deficient HL-1 (PKP2) were kindly provided by Dr. Marian and his group at UTHealth (Houston, Texas, US) [185,186]. Both HL-1 cell lines were cultured according to the protocol established by Claycomb and colleagues [187]. Briefly, cells were seeded on substrates previously coated with 0.005% fibronectin and 0.02% gelatin. HL-1 were cultured in Claycomb medium supplemented with 2mM L-glutamine, 10% fetal bovine serum, 100 U/ml penicillin, 100 µg/ml streptomycin and 10 mM norepinephrine; all chemicals were purchased from Sigma-Aldrich. Cell cultures were maintained according to standard procedures in a humidified incubator at 37°C, 5% CO_2.

3.1.2 DCM/*FLNC* framework

hiPSC-CMs were kindly provided by Dr. Mestroni and her group at University of Colorado Denver (Aurora, Colorado, US). Four conditions were studied: one was a commercial line derived from foreskin (identified in this work as "4skin"); one was derived from a patient ("MC166"); the last two were generated from "MC166" by CRISPR/Cas9 gene-editing to obtain $FLNC^{KO+/-}$ and $FLNC^{KO-/-}$ hiPSCs (identified as "FLNC Het" and "FLNC Homo"). Cells were cultured and differentiated into cardiomyocytes according to the protocol established by Sharma et al., which results in a purified cardiomyocyte population after 17 days of culture [Sharma et al., 2015]. Simply, hiPSCs were differentiated into cardiomyocytes by chemically modulating the Wnt/ß-catenin signaling through CHIR and IWR molecules. Then, hiPSC-CMs were further purified following glucose starvation. As well as HL-1, hiPSC-CMs were maintained in a humidified atmosphere at 37°C, 5% CO_2.

3.1.3 HGPS/*LMNA* framework

Rat cardiac fibroblasts were isolated from neonatal, juvenile, and adult animals. The animal studies were in accordance with the guidelines of the University of Colorado Denver Animal Care and Use Committee.

Neonatal rat cardiac fibroblasts (NRCFs) were isolated from 1-3 days old Wistar rat pups as previously done by our research group [188]; the procedure was early described by Martinelli et al., but minor modifications were introduced [189]. Briefly, hearts were dissociated in CBFHH (calcium and bicarbonate-free Hanks with Hepes) buffer containing 0.5 mg/ml of Collagenase type 2, and 1 mg/ml of Pancreatine. Fibroblasts were separated from cardiomyocytes plating the cellular suspension on a 100-mm Petri dish.

After 45 minutes, the supernatant containing cardiomyocytes was removed, leaving fibroblasts on the bottom. NRCFs were cultured in Dulbecco's Modified Eagle Medium (DMEM) high glucose, supplemented with 10% fetal bovine serum, heat inactivated and 1% antibiotic-antimycotic. Cells were maintained in a humidified incubator at 37°C, 5%CO_2 and passaged until P7.

Juvenile and adult rat cardiac fibroblasts (JRCFs and ARCFs, respectively) were kindly provided by Dr. Kathleen Woulfe and Cortney Wilson at University of Colorado Denver. Notably, ARCFs were isolated from female rats only, whereas NRCFs and JRCFs were both genders. Concisely, hearts were perfused and digested to obtain a myocytes pellet. The supernatant containing fibroblasts was centrifuged at 400g for 10 minutes to separate the fibroblasts. JRCFs and ARCFs were cultured according to the conditions previously described for NRCFs.

3.2 Infection of NRCFs, JRCFs, and ARCFs with adenoviral vectors

The adenoviral vectors (AdV) used in this study were kindly provided by Dr. Mestroni (UCDenver). The *LMNA* mutation studied in this work was G608G. AdVs were generated with the same method previously reported by our group [61]. Briefly, the hLMNA (wild type and mutant) cDNA was cloned into the Dual CCM plasmid (shuttle vector) and delivered into the Adenovirus vector through homologous recombination using the Gateway® technology. The pAd vector is a bicistronic adenovirus vector that contains GFP as a tag marker 5' to hLMNA. The inserts (EGFP and LMNA) were regulated by CMV promoters. Therefore, cells expressing hLMNA can be identified using GFP as a marker of infection.

NRCFs, JRCFs, and ARCFs were starved for at least 40 minutes before infection, followed by adenoviral infection at 50 multiplicity of infection (MOI). Cells were kept overnight in complete medium at 37°C, 5% CO_2. 24 hours after infection, medium was replaced with fresh complete medium. All experiments were performed 48 hours after infection, according to the protocol previously established in our laboratory [61,190].

3.3 Immunofluorescence experiments

In the frameworks where IF experiments were required, cells were fixed for 15 minutes with 4% paraformaldehyde (ThermoFisher Scientific).

For vimentin staining, cells were blocked for 1 hour with 5% donkey serum in 1X phosphate buffer saline (PBS)/0.3% Triton X-100. Cells were stained overnight at 4°C with 1:500 primary antibody against vimentin (ab137321, abcam). After rinsing with PBS 1X, cells were incubated for 1 hour at room temperature with 1:1000 secondary antibody (A-11035, Invitrogen). Representative images were acquired using DFC450 C (Leica).

For actin staining, cells were permeabilised for 5 minutes with 1X PBS/0.3% Triton X-100. Then, cells were incubated for 30 minutes at room temperature with 1X PBS/0.3% Triton X-100/1% bovine serum albumin (BSA). 5 μl of phalloidin staining solution (Texas Red™-X Phalloidin, ThermoFisher

Scientific) were added to 200 µl of 1X PBS, and then placed on the samples for 20 minutes at room temperature, according to the manufacturer's recommended protocol. Representative images were acquired using EVOS FL Cell Imaging System (ThermoFisher Scientific).

In fixed cells, nuclei were counterstained with 1:8000 DAPI (D1306, ThermoFisher Scientific).

Living NRCFs, JRCFs, ARCFs, and hiPSC-CMs probed via AFM were stained with a cell-permeant nuclear counterstain (NucBlue™, ThermoFisher Scientific). Cells were incubated with the staining solution for at least 20 minutes at 37°C, according to the manufacturer's instructions.

3.4 AFM sample preparation

3.4.1 AC/*PKP2* framework

For AFM experiments, WT and PKP2 HL-1 cells were seeded on borosilicate circular coverslips (Ø = 24 mm, thickness = 0.08 - 0.12 mm, Menzel Gläser). The coverslips were previously sonicated in 70% ethanol, dried under N_2, cleaned with oxygen plasma (GaLa Instrumente), and then coated with 0.005% fibronectin and 0.02% gelatin (Sigma Aldrich). After dislodgement with TrypLE™ (ThermoFisher Scientific) and centrifugation according to [187], 70,000 cells were plated on each coverslip, then kept overnight in supplemented Claycomb medium at 37°C, 5% CO_2. 24 hours after plating, samples were probed by AFM.

3.4.2 DCM/*FLNC* framework

FLNC hiPSC-CMs were plated on 35 mm-culture plates (93040, TPP) 5 days prior to AFM measurements. Briefly, hiPSC-CMs were trypsinised and individualised using TrypLE® (Gibco) according to the manufacturer's recommended protocol. Approximately 100,000 hiPSC-CMs were plated on Matrigel coated plates. The hiPSC-CMs were allowed to recover for a minimum of three days prior to experiments. hiPSC-CMs were observed every for signs of contraction. hiPSC-CMs that were not beating after 5 days in culture were discarded.

3.4.3 HGPS/*LMNA* framework

For AFM experiments, NRCFs, JRCFs, and ARCFs were seeded in 35 mm-Petri dishes (93040, TPP), previously coated with 0.1% porcine gelatin (Sigma Aldrich). In brief, cells were dislodged with 1X Trypsin EDTA (Sigma Aldrich), centrifuged at 220g for 3 minutes, and 50,000 cells were taken to be plated in each Petri dish. The day after seeding, cells were infected as previously described. AFM experiments were performed 48 hours after administration of the adenoviral constructs, in accordance with the protocol established by [61,190].

3.5 AFM experiments

Force spectroscopy experiments on HL-1 cells were carried out at BOKU University (Vienna, Austria) by using a NanoWizard® II (JPK Instruments), whereas tests on primary cardiac fibroblasts and hiPSC-CMs were performed at UCDenver (Aurora, Colorado, US) with a NanoWizard® 4a (JPK Instruments). In both cases, AFM was mounted on an inverted optical microscope (Zeiss) to visualise cells during experiments.

Every measurement was acquired on single, living, and intact cells in appropriate medium. The cell status was monitored during the experiment by using the optical microscope coupled with the AFM. Single cells were selected based on comparable morphology to minimise data variability.

3.5.1 AC/*PKP2* framework

WT and PKP2 HL-1 cells were tested at 37°C using the BioCell™ liquid chamber (JPK Instruments) (Figure 13), coupled with the CellHesion® module (JPK Instruments). All experiments were carried out in complete Claycomb medium. The duration of the experiments was limited to minimise the effects of pH changes in the cell medium.

F-d curves were acquired with DNP-S10 probes (Bruker), which are made of a silicon nitride cantilever and a sharpened tip (Figure 13). In each set of experiments, cantilevers were calibrated using the thermal noise option provided in the JPK software. The resulting spring constant was usually around 0.175 N/m.

Control and mutant cells were probed at one position corresponding to the nuclear region.

The maximum load applied was 4 nN. Dwell time was set at 60 s, and the loading rate (approach and retraction speed) was 10 μm/s.

3.5.2 DCM/*FLNC* framework

4SKIN, MC166, FLNC Het, and FLNC Homo cells were tested at 37°C using the PetriDishHeater™ liquid chamber (JPK Instruments) (Figure 14). All experiments were carried out in RPMI medium supplemented with Insulin. As well as tests on HL-1, the duration of the experiments was limited to minimise the influence of pH variations on the samples.

F-d curves were acquired with CP-PNP probes (NanoAndMore), which are made of a silicon nitride cantilever and a Pyrex-nitride spherical probe (Figure 14). According to the manufacturer, the sphere diameter is within the range 5.5 ÷ 9 µm, and was individually measured via optical microscopy before any experiment. In each set of measurements, cantilevers were calibrated using the thermal noise option provided in the JPK software. The resulting spring constant was around 0.03 N/m.

As already mentioned, cells were stained with NucBlue™ at least 20 minutes before the beginning of an experiment. Each cell was probed in its nuclear region, at a single position.
The maximum load applied was set at 2 nN, and loading rate at 2 μm/s.

3.5.3 HGPS/*LMNA* framework

NT, WT, and PRG cells were tested at 37°C using the PetriDishHeater™ liquid chamber (JPK Instruments) (Figure 14). All experiments were carried out in complete DMEM. Precautions were adopted in determining the duration of a batch of experiments, as reported in the previous frameworks. Force spectroscopy tests were performed with the same type of tip-cantilever assembly used for hiPSC-CMs (CP-PNP, NanoAndMore).
The spring constant, as calibrated with the JPK software, was around 0.05 N/m.
The experimental parameters were the same established for hiPSC-CMs.

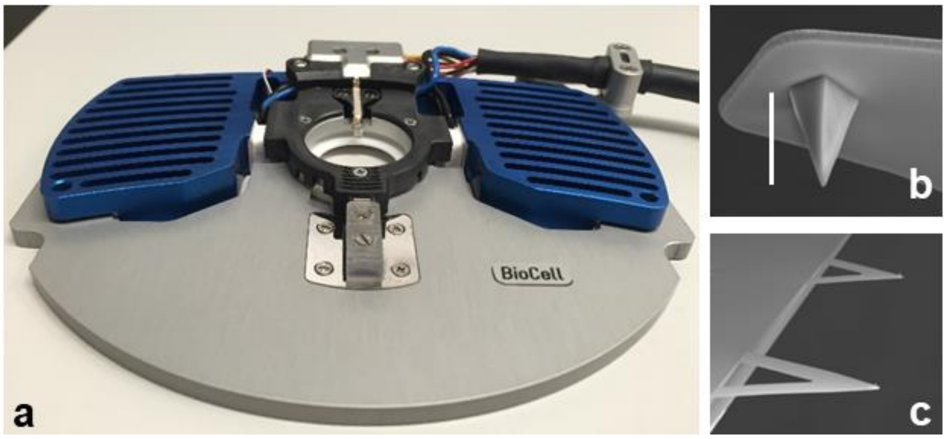

Figure 14 *AFM setup for measurements on HL-1 cells. BioCell™ chamber was used to maintain stable the temperature at 37°C (panel a). Cells were probed with a four-sided pyramidal tip (panel b), mounted on a triangular cantilever (panel c)* [191]*. White bar ranges within 2.2-8 um.*

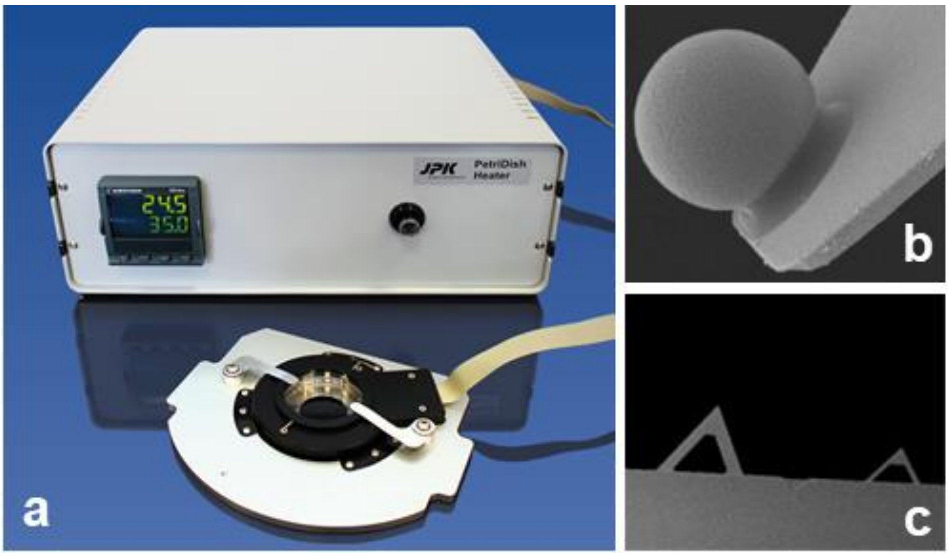

Figure 15 *AFM setup for measurements on cardiac fibroblasts and hiPSC-CMs. PetriDishHeater™ was used to maintain stable the temperature at 37°C (panel a). Cells were probed with a spherical tip (panel b), mounted on a triangular cantilever (panel c)* [192,193].

3.6 Stiffness and adhesion data analysis

F-d curves were analysed with the dedicated option in JPK software for assessing Young's modulus. Approach segments were fitted with the Hertz-Sneddon model implemented in the software, depending on the shape of the tip (either four-sided pyramid or sphere). Sample Poisson ratio was assumed to be 0.5, modeling cells as incompressible bodies [57,194]. Curves were fitted up to a pre-set value, varying from cell type to cell type, in order to maintain the measurements within 10% of the cell height and limit the effects of the hard substrate (refer to the introduction for motivations).

Adhesive properties of the cells were calculated from the retract segment of F-d curves, applying the options provided by JPK software.

3.7 Nuclear shape descriptor (circularity) assessment

In the LMNA framework, a nuclear shape descriptor was assessed by using ImageJ (version 1.51K). Briefly, an ImageJ-based threshold extraction method was used on the images acquired while performing AFM experiments. Cell nuclei were described in terms of circularity, as follows:

- circularity is defined as 4*π*area/(perimeter^2), and ranges from 0.0 to 1.0, with 1.0 representing a perfect circle.

3.8 Statistical analyses

Experimental AFM data were analysed using GraphPad Prism (GraphPad Software, Inc). Data are represented as boxplots in the style of Tukey. These plots visualise summary statistics (median, hinges, and fences) and individual outlying points. The horizontal line represents the second quartile (median), whereas hinges correspond to the first and third quartiles. The upper fence extends from the third quartile to the greater value, no further than (3rd quartile + 1.5*IQR), where IQR is the interquartile distance. The lower fence ranges from the 1st quartile to the lowest value, at most 1.5*IQR of the hinge.
Data normality was verified by Shapiro-Wilk test.
WT and PKP2-deficient HL-1 cells were analysed with Kruskal-Wallis and Mann-Whitney-Wilcoxon tests since distributions were found to be not normal. In other frameworks, where not normal distributions were found, Kruskal-Wallis test was applied, followed by Dunn's multiple comparisons test, in accordance with [61].
Shape descriptors data were analysed as well as AFM data.
In all instances, a significance $\alpha = 0.05$ level was assumed.

Chapter 4: Results and Discussion

4.1 AC/*PKP2* framework

Wild-type (WT) and PKP2-deficient (PKP2) HL-1 cells were probed with a four-sided pyramidal tip, and F-d curves were subsequently analysed for studying AC.

4.1.1 Stiffness

Approach segments of F-d curves were fitted up to 500 nm and 1 μm, which were consistent with cell heights previously measured by our research group (manuscript submitted for publication). Figure 15 shows the boxplots for Young's modulus, as calculated from the different fittings.

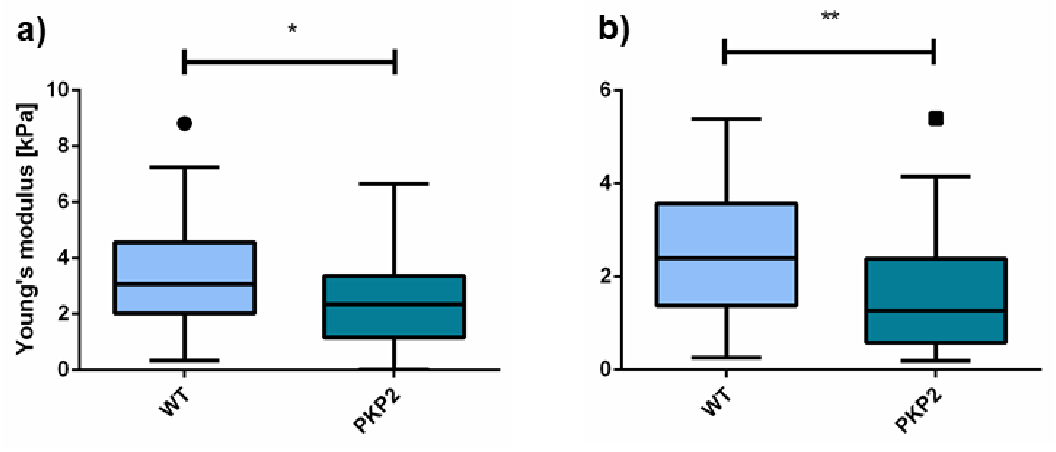

Figure 16 *Panel a) shows the Young's modulus as calculated from Hertz-Sneddon model, with a fitting range of 500 nm ($n^{WT}=30$; $n^{PKP2}=35$). Panel b) represents Young's modulus when the fitting extends to 1 μm ($n^{WT}=35$; $n^{PKP2}=45$). Mann-Whitney-Wilcoxon rank sum test showed significant difference between WT and PKP2 (* p-value<0.05, **p-value<0.01).*

Regardless of the fitting used, Young's modulus of PKP2-deficient cells was always lower than wild-type HL-1 cells. This is in accordance with the data previously reported by our research group: mutant cells were shown to have a nuclear stiffness 5-times lower than wild-type counterpart [195]. Although, in our previous works, a different setup was used, namely cell nuclei were probed with a spherical probe, at 1 μm/s, and F-d curves were fitted up to 1 μm (manuscript submitted for publication). The trend observed was comparable, but the absolute values we hereby measured were higher than those reported in the manuscript submitted for publication. Young's modulus of wild-type HL-1 cells was also higher than the value of HL-1 cells assessed by Kossivas and colleagues with a sphere-shaped cantilever tip [196]. Actually, this is consistent with literature: sharp tips usually detect higher stiffness than spherical probes.

For instance, Rico and coworkers found greater Young's modulus of epithelial A549 cells by using blunted pyramidal tips than spherical probes [197]. Similarly, sharp tips yielded higher stiffness of both HUVEC and Schlemm's canal cells than spherical tips [198].

Despite the difference observed between sharp and spherical probes remains an intriguing and controversial issue, it goes beyond the scope of this thesis. What is important to stress is that our experimental setup was able to detect a significant difference in the stiffness of wild-type and mutant cells, thus proving the power of AFM. The variation we observed is consistent with PKP2 deficiency, which is known to cause major alterations in cytoskeletal actin [199] and impair desmosomes disrupting desmoplakin assembly dynamics [200]. Further experiments would be required, but AFM assessment of Young's modulus certainly directs the future investigations towards cytoskeleton and nucleus, thus the key players in regulating cell stiffness.

4.1.2 Adhesion

The following figure is representative of the adhesive properties of WT and PKP2 HL-1 cells, as measured from the retraction segment of F-d curves.

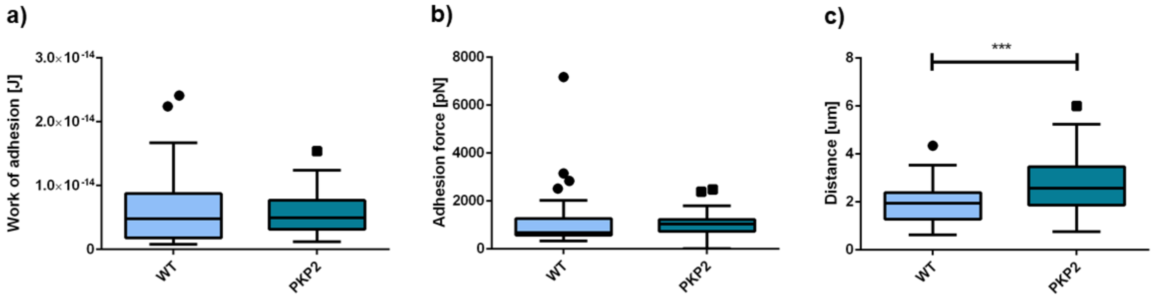

Figure 17 *Panels a), b), and c) refer to work of adhesion, adhesion force, and distance at which the adhesion force occurs, respectively. Mann-Whitney-Wilcoxon rank sum test highlights a significant difference between WT and PKP2 only in the distance dataset (*$n^{WT}=40; n^{PKP2}=39$*) (*** p-value<0.001).*

Interestingly, our data differed from the results found by Puzzi et al. in 2015 [195]: while they detected a significant difference in the work of adhesion, we did not. This is most likely due to the different setup, since we used a four-sided pyramidal tip instead of a spherical probe. The contact area between tip and sample was therefore different (greater in the case of the sphere), and it is reasonable to speculate that more interactions may take place if a larger area is available. We tried to act on the dwell time, increasing it up to 60 s, in order to promote the interaction between tip and cell. Nonetheless, no variation occurred in work of adhesion and adhesion force between WT and PKP2 cells. Conversely, a significant change was detected in the distance at which the maximum adhesion force occurs. Notably, we observed a decrease in the Young's modulus of mutant cells, and the corresponding increase of the distance. We can therefore hypothesise that the distance at which the tip starts to detach from the cell may be higher because the cell is more deformable (i.e. with lower stiffness). To the best of our knowledge, this interesting result has never been observed and discussed in any biological event thought to impair mechanical properties. We would suggest further investigations to identify the major contributors to this phenomenon, either cytoskeleton or nucleus; since one of the properties involved is cell stiffness, most likely the variation is related to these elements. This goal could be achieved by selectively inhibit certain elements, like actin or microtubules (i.e. administration of cytochalasin D or nocodazole).

4.2 DCM/*FLNC* framework

hiPSC-CMs derived from the commercial line (4skin), the donor (MC166), and the gene-edited cells (FLNC Het and FLNC Homo) were indented with a spherical probe to obtain F-d curves and investigate DCM phenotype *in vitro*.

4.2.1 Stiffness

Approach segments of F-d curves were fitted up to 400 nm. This value is consistent with the cell height revealed by AFM imaging, which was around 4 µm at its minimum (data not shown). Figure 17 shows the boxplots for Young's modulus.

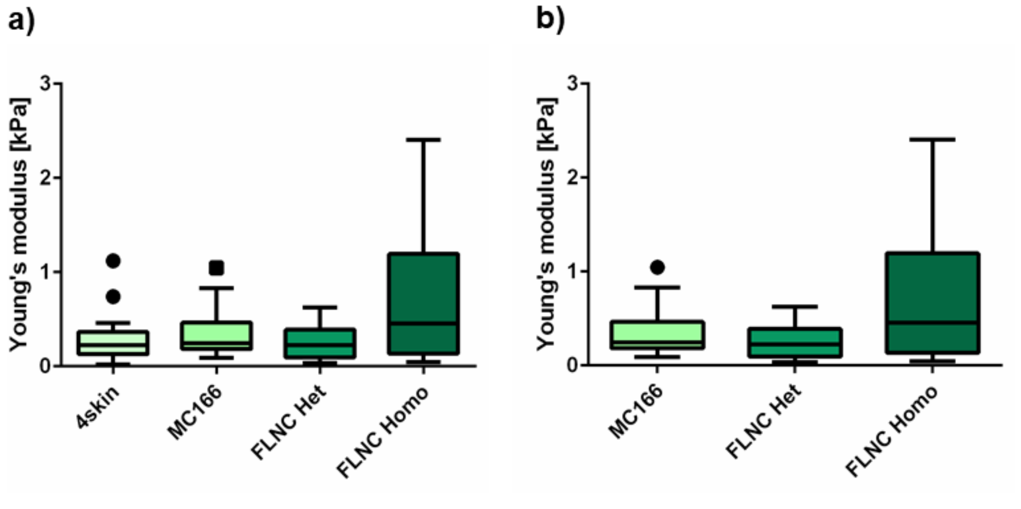

Figure 18 *Panel a) shows the Young's modulus calculated for cardiomyocytes derived from a commercial line (foreskin, "4skin"), hiPSCs from a patient ("MC166"), and from CRISPR-CAS9-edited MC166 ("FLNC Het" and "FLNC Homo"). Panel b) focuses on the isogenic data. Kruskal-Wallis test, followed by Dunn's test, does not find a significant difference among the groups* ($n^{4skin}=21$; $n^{MC166}=16$; $n^{FLNC\ Het}=28$; $n^{FLNC\ Homo}=18$).

One of the major contributor to cell stiffness, the cytoskeleton, was stained for actin in randomly selected samples: actin staining was thus performed on the commercial line-derived cardiomyocytes and the FLNC heterozygous specimens. Experiments showed a different actin organisation in the samples, with the controls exhibiting the typical striated structure of cardiomyocytes. This was not detected in the heterozygous specimen. Representative images follow (Figure 18):

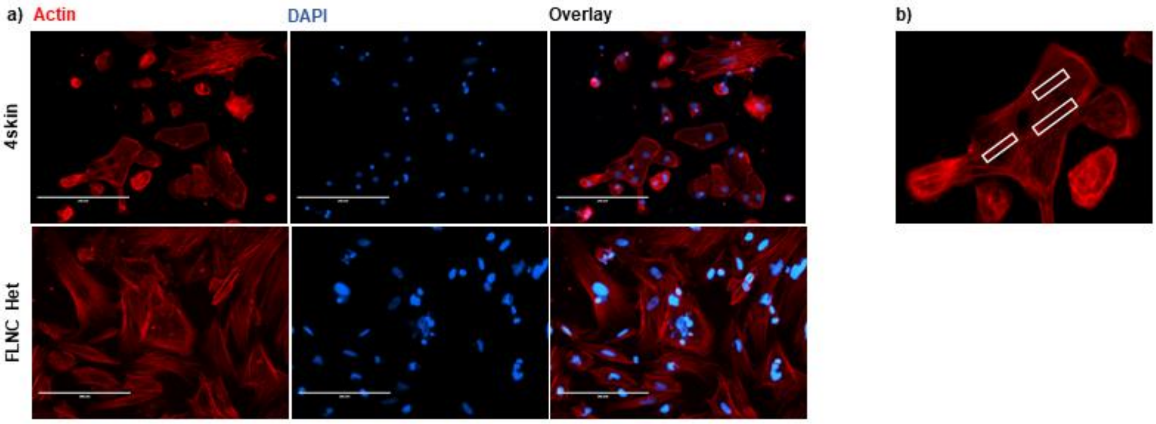

Figure 19 *Panel a) shows the actin staining (red) for 4skin and FLNC Het cells. Typical striated structure of cardiomyocytes is observed in controls (white boxes), as in the magnification provided in panel b). Scale bar: 200 µm.*

Since filamin C is known to be an actin-binding protein, the altered actin organisation is most likely due to the partial deletion of this protein in FLNC Het cells. Nonetheless, AFM was not able to detect a significant variation of cell stiffness. Our observations may be affected by the sample size, which is sufficient, but could be improved. Increasing the number of data could reduce the variability observed, above all, in FLNC Homo dataset and may potentially change the conclusions hereby reported.

Besides, it is worth mentioning that cytoskeleton is a key player in providing strength to the cell, but nucleus is pivotal too. In order to prevent artefacts due to substrate stiffness, all the measurements were performed above the nuclear region, which corresponds to the highest portion of a cell. Perhaps, the lacking detection of a variation in cell stiffness is caused by the contribute of the nucleus, which overcomes that of cytoskeleton (and actin, in particular). Further experiments may be carried in wider areas, exceeding the nucleus, to estimate “single” contributes.

4.2.2 Adhesion

The following figure is representative of the adhesive properties of hiPSC-CMs, as measured from the retraction segment of F-d curves.

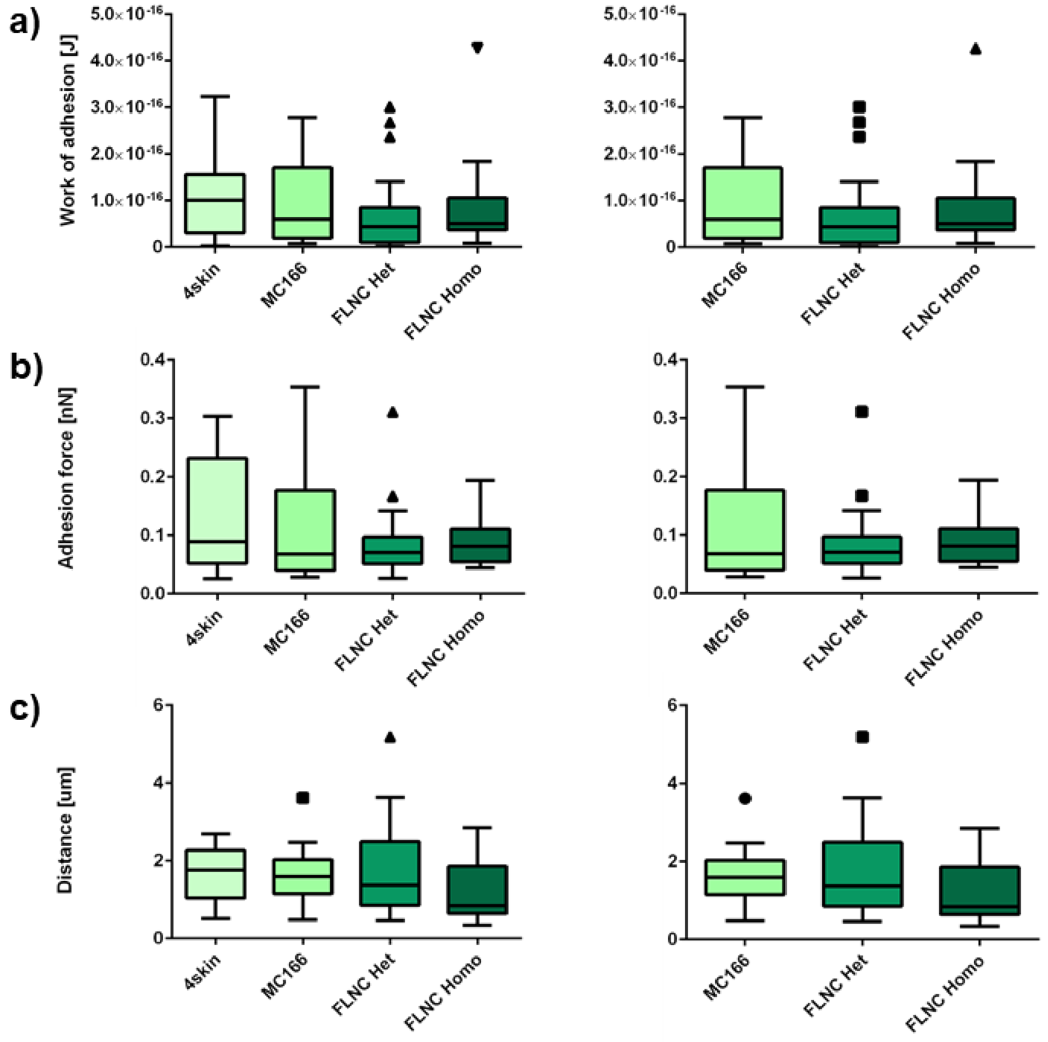

Figure 20 Adhesive properties of hiPSC-CMs as measured by AFM. Panels a), b), c) show the work of adhesion, adhesion force and distance at which the maximum force occurs, respectively. In each panel there are two boxplots, one comprising all the groups (4skin, MC166, FLNC Het, FLNC Homo), whereas the other includes only the isogenic data (MC166 and the gene-edited groups FLNC Het and FLNC Homo). Kruskal-Wallis and Dunn's tests did not detect any significant difference among the groups ($n^{4skin}=15$; $n^{MC166}=10$; $n^{FLNC\ Het}=25$; $n^{FLNC\ Homo}=12$).

AFM analysis of adhesive properties of FLNC-deficient hiPSC-CMs did not reveal any significant difference among groups, despite filamin C being potentially involved in cell-cell and cell-ECM interactions. Our analysis might suffer from lack of data, so even in this case, further experiments are suggested. This type of experiment assesses nonspecific adhesive properties, and these are probably not susceptible to FLNC absence. Since filamin C interacts with integrins, AFM experiments with tips functionalised with ECM proteins could reveal alterations of specific adhesive mechanisms.

4.3 HGPS/*LMNA* framework

Once isolated and infected, cardiac fibroblasts were stained to verify the amount of fibroblasts. In literature, fibroblasts are often identified with antibodies against vimentin, an intermediate filament expressed in fibroblasts [201,202]. Majority of cells was positive for vimentin staining, as shown in the following representative images (Figure 20).

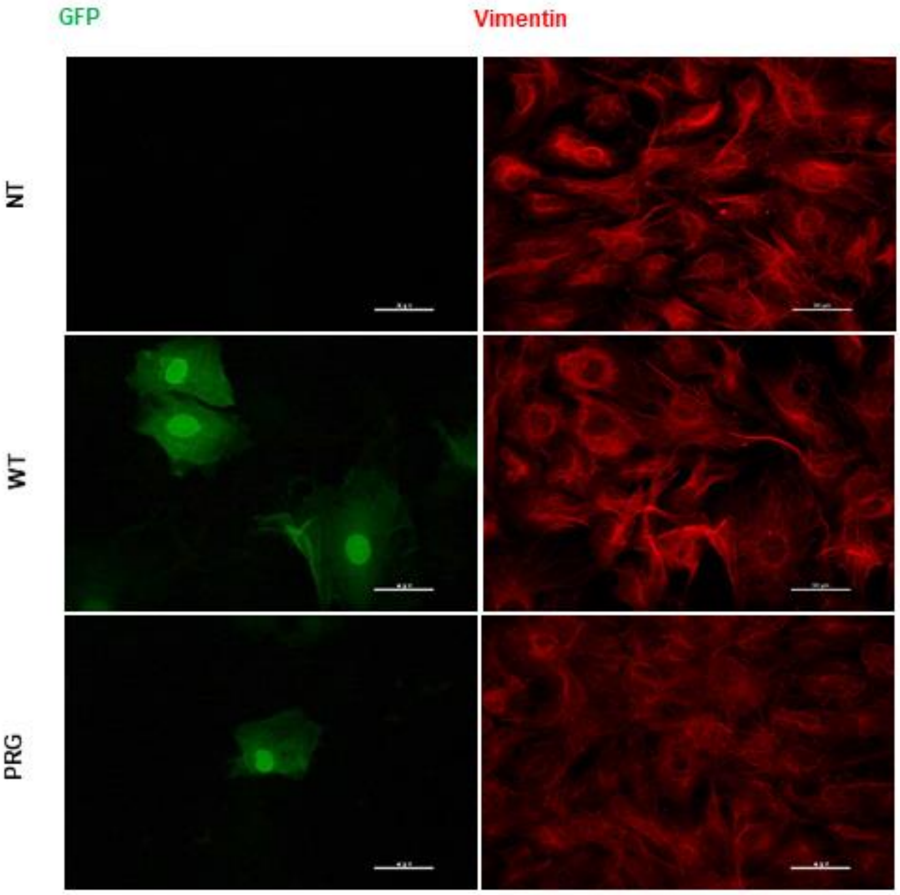

Figure 21 *Immunofluorescence staining for vimentin (red) as a marker for fibroblasts. GFP is associated with AdV expressing either wild-type (WT) or mutant (PRG) hLMNA. Most cells are positive for vimentin. Scale bar: 50 µm.*

Neonatal, juvenile, and adult cardiac fibroblasts were probed with a sphere-shaped tip, and F-d curves were subsequently analysed to elucidate the cell mechanical phenotype in HGPS.

4.3.1 Stiffness

Young's moduli of NRCFs, JRCFs, and ARCFs are presented in Figure 22. Approach segments of F-d curves were all fitted up to 200 nm because AFM imaging revealed an average cell height around 2 µm (data not shown).

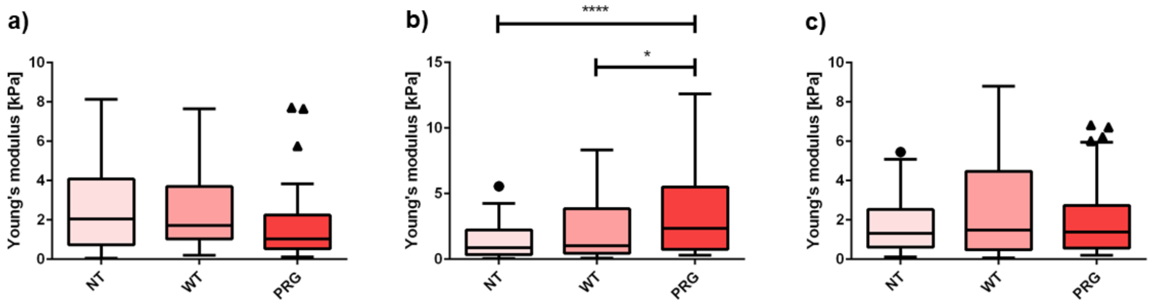

Figure 22 *Young's moduli of NRCFs (panel a), JRCFs (panel b), and ARCFs (panel c). Kruskal-Wallis and Dunn's tests found a statistical difference only between controls and PRG fibroblasts isolated from juvenile animals (NRCFs:* $n^{NT}=84$*;* $n^{WT}=43$*;* $n^{PRG}=36$*. JRCFs:* $n^{NT}=78$*;* $n^{WT}=44$*;* $n^{PRG}=42$*. ARCFs:* $n^{NT}=76$*;* $n^{WT}=45$*;* $n^{PRG}=49$*.) (* p-value<0.05; **** p-value<0.0001).*

Even if detected only in cells from juvenile rats, the increase of cell stiffness due to mutant hLMNA is in accordance with literature. Mutations associated with HGPS have been previously shown to cause higher Young's moduli. For example, we already anticipated that ectopically expression of mutant (E145K) lamin in *Xenopus* oocytes caused an increase of Young's modulus of isolated nuclei, when measured by AFM and compared to controls [181]. Similarly, AFM assessed a higher nuclear stiffness in dermal fibroblasts from a patient bearing the E145K mutation than young and old donors [182].

Conversely, no significant difference was measured in NRCFs. This leads to speculate that the effect of G608G LMNA on cell stiffness follows an age-dependent trend. The relationship should be confirmed in the ARCFs, but no statistical difference among the groups in cells from adults was detected. Nevertheless, it is crucial to remind that ARCFs were isolated from females only, whereas NRCFs and JRCFs are mixed populations. These results suggest that Young's modulus could be influenced by gender in this *in vitro* model. *De facto*, a male to female ratio of 1.2:1 was reported in literature by Hennekam, thus there is a slightly higher number of male HGPS patients compared to females [162]. These data raise interest, but first the dataset of ARCFs shall be extended to male rats to confirm the relationship between cell stiffness and age.

Given the statistical difference in JRCFs, we stained actin to compare its organisation between wild-type and mutant cells. Representative images are hereby reported:

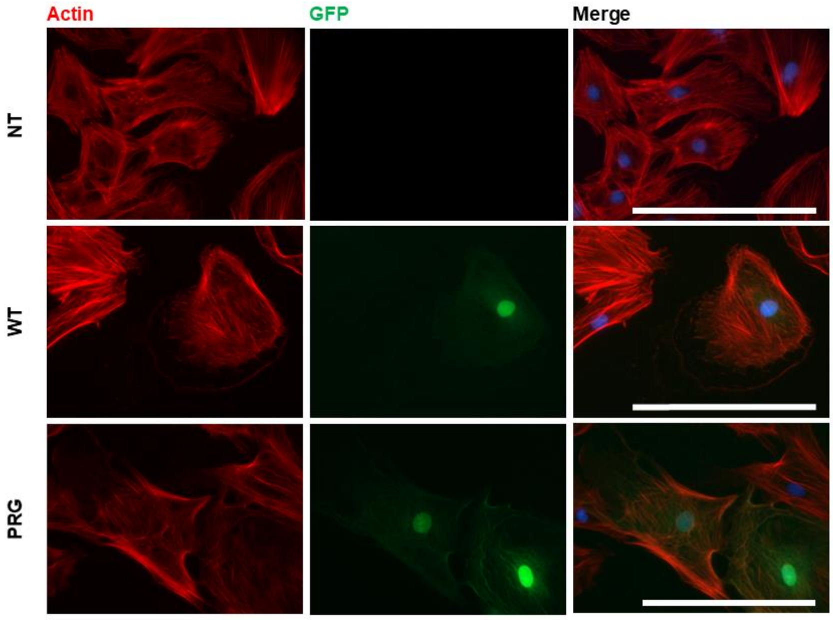

Figure 23 *Immunofluorescence staining for actin (red). GFP is associated with AdV expressing either wild-type (WT) or mutant (PRG) hLMNA. Scale bar: 200 µm.*

Since no clear evidence of a different actin assembly was found, and lamin A/C is localised in the nucleus, we compared the nuclear shape of controls and mutant cells. Circularity of nuclei was assessed via an ImageJ-based threshold extraction method and analysed as well as AFM data.

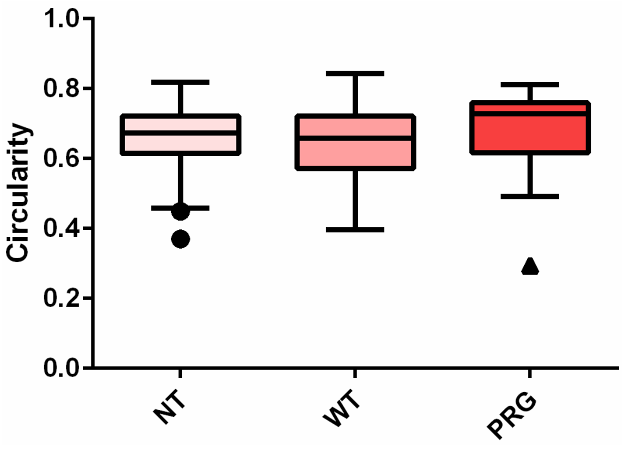

Figure 24 *Kruskal-Wallis test, followed by Dunn's test, did not reveal a significant difference among the groups in JRCFs. Therefore, nuclear shape is assumed to be identical between controls and mutant cells, despite the presence of G608G lamin* ($n^{NT}=72$; $n^{WT}=42$; $n^{PRG}=41$).

Circularity of nuclei is assumed to be identical in NT, WT, and PRG JRCFs, because data analysis did not find any significant difference. This may be consistent with literature, since dermal fibroblasts from HGPS patients showed an increasingly abnormal nuclear shape when associated with the increase of passage number in culture [203]. Verstraeten et al. hypothesised that nuclear shape alteration was caused by the accumulation of abnormal lamin at the nuclear envelope [203]. Unfortunately, our system (adenoviral vector) does not provide a stable expression of mutant protein when cells proliferate; indeed, the mutation is not transferred to daughter cells, as it would be with a lentivirus. This *in vitro* model may be not appropriate for a long-term study of the nuclear shape, nonetheless proved to be effective in discerning the mechanical properties of cells bearing the mutation. Further investigations are required to identify the mechanisms responsible for the variation of cell stiffness: in particular, it is mandatory to find out an eventual correlation with age and sex of the animal model, as was suggested by our findings.

4.3.2 Adhesion

Nonspecific adhesive properties of NRCFs, JRCFs, and ARCFs were assessed from the retract segments of F-d curves. Data are presented in the following:

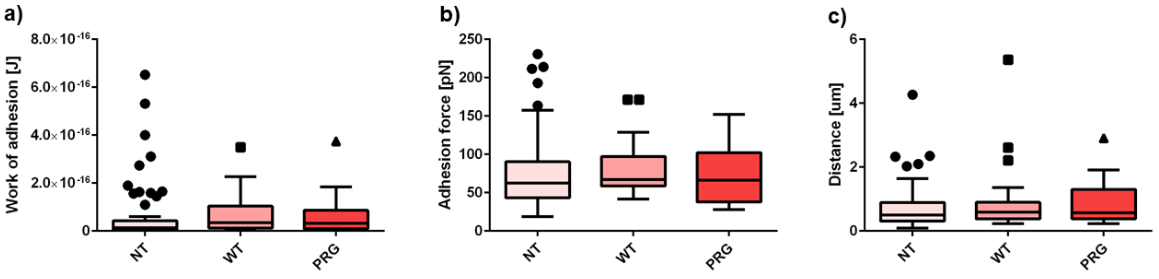

Figure 25 *Adhesive properties of NRCFs: work of adhesion (panel a), adhesion force (panel b), and distance at which the adhesion force occurs (panel c). Kruskal-Wallis and Dunn's tests did not reveal a statistical difference among the groups for every parameter (NRCFs: $n^{NT}=60$; $n^{WT}=33$; $n^{PRG}=28$).*

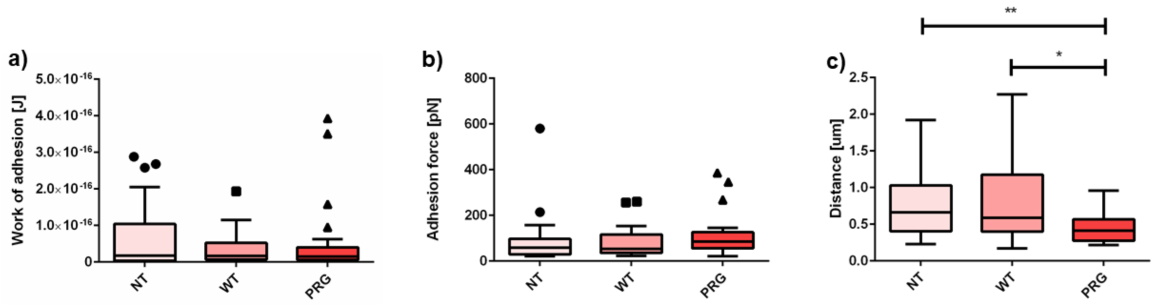

Figure 26 *Adhesive properties of JRCFs: work of adhesion (panel a), adhesion force (panel b), and distance at which the adhesion force occurs (panel c). Kruskal-Wallis and Dunn's tests found a statistical difference among the groups only for the distance (JRCFs: $n^{NT}=43$; $n^{WT}=25$; $n^{PRG}=25$) (* p-value<0.05; ** p-value<0.01).*

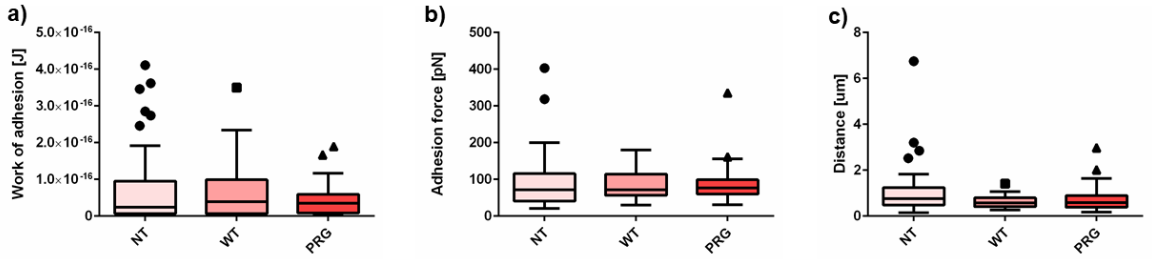

Figure 27 *Adhesive properties of ARCFs: work of adhesion (panel a), adhesion force (panel b), and distance at which the adhesion force occurs (panel c). Kruskal-Wallis and Dunn's tests did not find a significant difference among the groups for every parameter (ARCFs:* $n^{NT}=45$*;* $n^{WT}=21$*;* $n^{PRG}=32$*).*

Only in JRCFs, data analysis revealed a significant difference in one property, namely the distance at which the maximum adhesion force occurs. In particular, distance decreased in PRG cells, which simultaneously experienced an increase of the Young's modulus (paragraph 4.3.1). Hence, the harder the cell becomes because of the genetic mutation, the shorter the distance can be. This result strengthens the trend observed in wild-type and PKP2-deficient HL-1 cells. In those cells, there was an increase in the Young's modulus, associated with a reduction of the distance. Taken together, these data suggest a link between Young's modulus and distance, which is a novel finding in the field of AFM applied to living cells. Even in this case, it would be necessary to identify the cellular elements responsible for the behaviour observed. Although, the fact that LMNA is localised to the nucleus supports our speculation (i.e. a major involvement of cytoskeleton and nucleus).

Chapter 5: Conclusions

In this thesis, we provided evidence that genetic diseases can be successfully studied from a mechanical point of view. We investigated three different diseases, which mainly affect the heart: AC, DCM, and HGPS. We focused our efforts on three disease genes, namely *PKP2* for AC, *FLNC* for DCM, and *LMNA* for HGPS. We induced either suppression or mutation of these genes and studied their effects on the mechanical behaviour of cells via AFM.

PKP2-deficient HL-1 cells have been found softer than wild-type. Interestingly, we discovered that mutant cells exhibited a higher distance at which the maximum adhesion force occurs. The relationship between variation of cell stiffness and alteration of the distance was observed also in the *in vitro* progeria model, specifically in cardiac fibroblasts isolated from juvenile rats. When infected with an AdV carrying G608G LMNA mutation, JRCFs had higher Young's modulus and reduced distance respect to controls. In all the other frameworks, the mechanical properties we measured did not vary between controls and mutant samples. A summary of our findings is shown in the following table:

Disease (Gene)	**Cellular model**	**Young's modulus**	**Work of adhesion**	**Adhesion force**	**Distance**
AC (*PKP2*)	HL-1	↓	—	—	↑
DCM (*FLNC*)	hiPSC-CMs	—	—	—	—
HGPS (*LMNA*)	NRCFs	—	—	—	—
	JRCFs	↑	—	—	↓
	ARCFs	—	—	—	—

Table 2 *Summary of the results obtained within this thesis. The arrows indicate a variation in the mechanical properties. Up direction represents an increase of the value between mutant samples and controls, whereas down direction means a reduction. Dash indicates no variation occurring.*

The alterations we observed in two out of three frameworks (AC/*PKP2* and HGPS/*LMNA*) confirm our hypotheses that some genetic mutations can impair the overall cell status, and mechanical features are crucial to completely understand a pathologic phenotype. Our data demonstrate that AFM is a powerful toolbox to study the mechanical properties of cells in *in vitro* models of genetic diseases. In the future, biomechanical properties could potentially become the cornerstone for novel medical approaches to genetic diseases, mimicking what has already been done for other types of health issues. For instance, Islam and colleagues developed a microfluidic device that sorts sensitive and drug-resistant leukemia cells based on the difference in their stiffness [204]. Another example is the engineered mechanoresponsive mesenchymal stem cells system that can act as vehicle for selective cancer drug delivery designed by Liu and coworkers [205]. Furthermore, cell mechanical properties have been suggested as innovative quality indicators for oocytes sorting before *in vitro* fertilisation procedures, and allowed the identification of new potential druggable targets for ovarian cancer [206,207]. In particular, human ovarian cancer cells (HEYA8 and OVCAR8) were transfected to overexpress five tumour-suppressor microRNAs, known to improve the clinical outcomes for this type of cancer [207]. Assessing the mechanical properties of these cells showed that the microRNAs alter cell mechanics by regulating the actin cytoskeleton, as well as the invasive behaviour of ovarian cancer cells [207]. Lastly, in the frame of cardiology, our group dosed a p38 MAPK inhibitor to rescue the mechanical properties of neonatal rat cardiomyocytes with *LMNA* mutations recognised to cause DCM. Indeed, p38 MAPK pathway has been proven to play a key role in many cardiac diseases, included DCM [61]. Drug administration rescued the cell mechanical behaviour and recovered the disrupted actin network, strengthening the view that AFM can be useful for innovative *in vitro* drug screening tests [61].

It is worth to emphasise again our discovery that Young's modulus and distance are likely to be associated in presence of a genetic mutation that causes the variation of one of these proerties. Actually, it seems that the more deformable the cell becomes, the more the cell can be stretched and pulled up by the AFM probe, and vice versa. To the best of our knowledge, this relationship has never been reported before, even for other types of diseases (e.g. cancer). This is an additional information we can derive from F-d curves and must foster future investigations to identify the causative agents. Certainly, a deep understanding of the roles of cytoskeleton and nucleus as major modulators of deformability would be a good starting point. These findings could provide further details about the link between the different mechanical properties, and eventually shed light on mechanotransduction mechanisms.

Despite the numerous advantages and promising results, AFM users must be aware of certain issues, like those that emerged throughout this work. Speed, force, and indentation depth must be carefully chosen, as well as tip geometry. Different tip shapes can lead to different results, in terms of both absolute values and trends, as we experienced with PKP2-deficient cells. Besides, consideration may want to be given to the position on the cell where measurements are performed. If probing the cell on the nuclear region can be a good practice, this may not reveal changes in the mechanical properties, as we observed in the case of FLNC-deficient cells. The FLNC framework also remarked that a good sample size is always beneficial. Nonetheless, the results we achieved on our FLNC samples must not draw a veil over the study of mechanical properties of cells lacking filamin C or bearing a mutant form. Supplementary experiments and integration of AFM data with other experimental procedures could provide novel insights.

At the end of this work, we can finally state that it was the intent of the author to encourage more researchers to venture into the realm of biomechanics on a regular basis; hopefully, this thesis provided its contribution to the cause.

Bibliography

1. Brand, R. A. Biographical Sketch: Julius Wolff, 1836–1902. *Clin. Orthop. Relat. Res.* **468**, 1047–1049 (2010).
2. Paluch, E. K. *et al.* Mechanotransduction: use the force(s). *BMC Biol.* **13**, (2015).
3. Engler, A. J., Sen, S., Sweeney, H. L. & Discher, D. E. Matrix Elasticity Directs Stem Cell Lineage Specification. *Cell* **126**, 677–689 (2006).
4. Liu, N. *et al.* Effect of substrate stiffness on proliferation and differentiation of periodontal ligament stem cells. *Cell Prolif.* **51**, e12478 (2018).
5. Gilbert, P. M. *et al.* Substrate Elasticity Regulates Skeletal Muscle Stem Cell Self-Renewal in Culture. *Science* **329**, 1078–1081 (2010).
6. http://www.who.int/news-room/fact-sheets/detail/cancer. Available at: http://www.who.int/news-room/fact-sheets/detail/cancer. (Accessed: 20th November 2018)
7. Denais, C. & Lammerding, J. Nuclear Mechanics in Cancer. in *Cancer Biology and the Nuclear Envelope* (eds. Schirmer, E. C. & de las Heras, J. I.) **773**, 435–470 (Springer New York, 2014).
8. Binnig, G., Quate, C. F. & Gerber, C. Atomic Force Microscope. *Phys. Rev. Lett.* **56**, 930–933 (1986).
9. Moreno Flores, S. & Toca-Herrera, J. L. The new future of scanning probe microscopy: Combining atomic force microscopy with other surface-sensitive techniques, optical microscopy and fluorescence techniques. *Nanoscale* **1**, 40 (2009).
10. Friedrichs, J. *et al.* A practical guide to quantify cell adhesion using single-cell force spectroscopy. *Methods* **60**, 169–178 (2013).
11. Benitez, R. & Toca-herrera, J. L. Looking at cell mechanics with atomic force microscopy: Experiment and theory: CELL MECHANICS WITH AFM. *Microsc. Res. Tech.* **77**, 947–958 (2014).
12. Martin, Y., Williams, C. C. & Wickramasinghe, H. K. Atomic force microscope–force mapping and profiling on a sub 100-Å scale. *J. Appl. Phys.* **61**, 4723–4729 (1987).

13. Rao, S. & Costa, K. D. Atomic Force Microscopy (AFM) in biomedical research. in *Biomedical Imaging* 41–64 (Elsevier, 2014). doi:10.1533/9780857097477.1.41
14. Hansma, H. G. *et al.* Recent advances in atomic force microscopy of DNA. *Scanning* **15**, 296–299 (1993).
15. Hansma, H. G., Kasuya, K. & Oroudjev, E. Atomic force microscopy imaging and pulling of nucleic acids. *Curr. Opin. Struct. Biol.* **14**, 380–385 (2004).
16. Lyubchenko, Y. L., Shlyakhtenko, L. S. & Ando, T. Imaging of nucleic acids with atomic force microscopy. *Methods* **54**, 274–283 (2011).
17. Kuznetsov, Y. G. *et al.* Atomic force microscopy imaging of retroviruses: Human immunodeficiency virus and murine leukemia virus. *Scanning* **26**, 209–216 (2006).
18. Martinez-Martin, D. *et al.* Resolving Structure and Mechanical Properties at the Nanoscale of Viruses with Frequency Modulation Atomic Force Microscopy. *PLoS ONE* **7**, e30204 (2012).
19. Kuznetsov, Y. G. & McPherson, A. Atomic Force Microscopy in Imaging of Viruses and Virus-Infected Cells. *Microbiol. Mol. Biol. Rev.* **75**, 268–285 (2011).
20. V. Dubrovin, E. AFM Specific Identification of Bacterial Cell Fragments on Biofunctional Surfaces. *Open Microbiol. J.* **6**, 22–28 (2012).
21. Jonas, K. *et al.* Roles of curli, cellulose and BapA in Salmonella biofilm morphology studied by atomic force microscopy. *BMC Microbiol.* **7**, 70 (2007).
22. Dufrene, Y. F. Atomic Force Microscopy in Microbiology: New Structural and Functional Insights into the Microbial Cell Surface. *mBio* **5**, (2014).
23. Hecht, E. *et al.* Combined Atomic Force Microscopy–Fluorescence Microscopy: Analyzing Exocytosis in Alveolar Type II Cells. *Anal. Chem.* **84**, 5716–5722 (2012).
24. Yoshida, A. *et al.* Morphological changes of plasma membrane and protein assembly during clathrin-mediated endocytosis. *PLOS Biol.* **16**, e2004786 (2018).
25. Li, M. *et al.* Atomic force microscopy imaging of live mammalian cells. *Sci. China Life Sci.* **56**, 811–817 (2013).
26. Gudzenko, T. & Franz, C. M. Studying early stages of fibronectin fibrillogenesis in living cells by atomic force microscopy. *Mol. Biol. Cell* **26**, 3190–3204 (2015).

27. Li, M., Liu, L., Xi, N. & Wang, Y. Nanoscale monitoring of drug actions on cell membrane using atomic force microscopy. *Acta Pharmacol. Sin.* **36**, 769–782 (2015).
28. Borin, D., Pecorari, I., Pena, B. & Sbaizero, O. Novel insights into cardiomyocytes provided by atomic force microscopy. *Semin. Cell Dev. Biol.* **73**, 4–12 (2018).
29. Hassenkam, T. *et al.* High-resolution AFM imaging of intact and fractured trabecular bone. *Bone* **35**, 4–10 (2004).
30. Raspanti, M. *et al.* The extracellular matrix of the human aortic wall: Ultrastructural observations by FEG-SEM and by tapping-mode AFM. *Micron* **37**, 81–86 (2006).
31. Pilarczyk, M. *et al.* Endothelium in Spots – High-Content Imaging of Lipid Rafts Clusters in db/db Mice. *PLoS ONE* **9**, e106065 (2014).
32. Graham, H. K. *et al.* Tissue section AFM: In situ ultrastructural imaging of native biomolecules. *Matrix Biol.* **29**, 254–260 (2010).
33. Yang, H., Liu, Y., Lu, X.-L., Li, X.-H. & Zhang, H.-G. Transmembrane transport of the Gαq protein carboxyl terminus imitation polypeptide GCIP-27. *Eur. J. Pharm. Sci.* **49**, 791–799 (2013).
34. Kliche, K. *et al.* Direct Aldosterone Action on Mouse Cardiomyocytes Detected with Atomic Force Microscopy. *Cell. Physiol. Biochem.* **18**, 265–274 (2006).
35. Dague, E. *et al.* Atomic force and electron microscopic-based study of sarcolemmal surface of living cardiomyocytes unveils unexpected mitochondrial shift in heart failure. *J. Mol. Cell. Cardiol.* **74**, 162–172 (2014).
36. Wang, L., Chen, T., Zhou, X., Huang, Q. & Jin, C. Atomic force microscopy observation of lipopolysaccharide-induced cardiomyocyte cytoskeleton reorganization. *Micron* **51**, 48–53 (2013).
37. Carvalho, F. A. & Santos, N. C. Atomic force microscopy-based force spectroscopy - biological and biomedical applications. *IUBMB Life* **64**, 465–472 (2012).
38. Moreno-Cencerrado, A. *et al.* Investigating cell-substrate and cell-cell interactions by means of single-cell-probe force spectroscopy: INVESTIGATING CELL ADHESION BY SINGLE CELL-PROBE AFM. *Microsc. Res. Tech.* **80**, 124–130 (2017).

39. Pfreundschuh, M., Martinez-Martin, D., Mulvihill, E., Wegmann, S. & Muller, D. J. Multiparametric high-resolution imaging of native proteins by force-distance curve–based AFM. *Nat. Protoc.* **9**, 1113–1130 (2014).

40. Thomas, G., Burnham, N. A., Camesano, T. A. & Wen, Q. Measuring the Mechanical Properties of Living Cells Using Atomic Force Microscopy. *J. Vis. Exp.* (2013). doi:10.3791/50497

41. Sirghi, L., Ponti, J., Broggi, F. & Rossi, F. Probing elasticity and adhesion of live cells by atomic force microscopy indentation. *Eur. Biophys. J.* **37**, 935–945 (2008).

42. Kuznetsova, T. G., Starodubtseva, M. N., Yegorenkov, N. I., Chizhik, S. A. & Zhdanov, R. I. Atomic force microscopy probing of cell elasticity. *Micron* **38**, 824–833 (2007).

43. Brückner, B. R. & Janshoff, A. Elastic properties of epithelial cells probed by atomic force microscopy. *Biochim. Biophys. Acta BBA - Mol. Cell Res.* **1853**, 3075–3082 (2015).

44. Chiang, M. Y. M., Yangben, Y., Lin, N. J., Zhong, J. L. & Yang, L. Relationships among cell morphology, intrinsic cell stiffness and cell–substrate interactions. *Biomaterials* **34**, 9754–9762 (2013).

45. Vinckier, A. & Semenza, G. Measuring elasticity of biological materials by atomic force microscopy. *FEBS Lett.* **430**, 12–16 (1998).

46. JPK. Available at: https://www.jpk.com/app-technotes-img/AFM/pdf/jpk-app-elastic-modulus.14-1.pdf. (Accessed: 20th November 2018)

47. Lekka, M. *et al.* Elasticity of normal and cancerous human bladder cells studied by scanning force microscopy. *Eur. Biophys. J.* **28**, 312–316 (1999).

48. Cross, S. E., Jin, Y.-S., Rao, J. & Gimzewski, J. K. Nanomechanical analysis of cells from cancer patients. *Nat. Nanotechnol.* **2**, 780–783 (2007).

49. Li, Q. S., Lee, G. Y. H., Ong, C. N. & Lim, C. T. AFM indentation study of breast cancer cells. *Biochem. Biophys. Res. Commun.* **374**, 609–613 (2008).

50. Xu, W. *et al.* Cell Stiffness Is a Biomarker of the Metastatic Potential of Ovarian Cancer Cells. *PLoS ONE* **7**, e46609 (2012).

51. Palmieri, V. *et al.* Mechanical and structural comparison between primary tumor and lymph node metastasis cells in colorectal cancer. *Soft Matter* **11**, 5719–5726 (2015).

52. Guo, X., Bonin, K., Scarpinato, K. & Guthold, M. The effect of neighboring cells on the stiffness of cancerous and non-cancerous human mammary epithelial cells. *New J. Phys.* **16**, 105002 (2014).
53. Kulkarni, A. H., Chatterjee, A., Kondaiah, P. & Gundiah, N. TGF- *β* induces changes in breast cancer cell deformability. *Phys. Biol.* **15**, 065005 (2018).
54. Cross, S. E., Jin, Y.-S., Lu, Q.-Y., Rao, J. & Gimzewski, J. K. Green tea extract selectively targets nanomechanics of live metastatic cancer cells. *Nanotechnology* **22**, 215101 (2011).
55. Yue, T. *et al.* Quantifying Drug-Induced Nanomechanics and Mechanical Effects to Single Cardiomyocytes for Optimal Drug Administration To Minimize Cardiotoxicity. *Langmuir* **32**, 1909–1919 (2016).
56. Zemła, J. *et al.* Atomic force microscopy as a tool for assessing the cellular elasticity and adhesiveness to identify cancer cells and tissues. *Semin. Cell Dev. Biol.* **73**, 115–124 (2018).
57. Lekka, M. *et al.* Erythrocyte stiffness probed using atomic force microscope. *Biorheology* **42**, 307–317 (2005).
58. Lekka, M., Fornal, M., Wizner, B., Grodzicki, T. & Styczen, J. Erythrocyte stiffness probed using atomic force microscope. 11
59. Dulińska, I. *et al.* Stiffness of normal and pathological erythrocytes studied by means of atomic force microscopy. *J. Biochem. Biophys. Methods* **66**, 1–11 (2006).
60. Benech, J. C. *et al.* Diabetes increases stiffness of live cardiomyocytes measured by atomic force microscopy nanoindentation. *Am. J. Physiol.-Cell Physiol.* **307**, C910–C919 (2014).
61. Laurini, E. *et al.* Biomechanical defects and rescue of cardiomyocytes expressing pathologic nuclear lamins. *Cardiovasc. Res.* **114**, 846–857 (2018).
62. Puzzi, L. *et al.* Cellular biomechanics impairment in keratinocytes is associated with a C-terminal truncated desmoplakin: An atomic force microscopy investigation. *Micron* **106**, 27–33 (2018).
63. Fletcher, D. A. & Mullins, R. D. Cell mechanics and the cytoskeleton. *Nature* **463**, 485–492 (2010).
64. Lammerding, J. Mechanics of the Nucleus. in *Comprehensive Physiology* (ed. Terjung, R.) (John Wiley & Sons, Inc., 2011). doi:10.1002/cphy.c100038

65. The Self-Assembly and Dynamic Structure of Cytoskeletal Filaments - Molecular Biology of the Cell - NCBI Bookshelf. Available at: https://www.ncbi.nlm.nih.gov/books/NBK26862/. (Accessed: 29th November 2018)
66. Lodish, H. *et al. Molecular Cell Biology*. (W. H. Freeman, 2000).
67. Cooper, G. M. & Cooper, G. M. *The Cell*. (Sinauer Associates, 2000).
68. Dahl, K. N. & Kalinowski, A. Nucleoskeleton mechanics at a glance. *J. Cell Sci.* **124**, 675–678 (2011).
69. Khalili, A. & Ahmad, M. A Review of Cell Adhesion Studies for Biomedical and Biological Applications. *Int. J. Mol. Sci.* **16**, 18149–18184 (2015).
70. Thiery, J. P. Cell adhesion in cancer. *Comptes Rendus Phys.* **4**, 289–304 (2003).
71. Thie, M. *et al.* Interactions between trophoblast and uterine epithelium: monitoring of adhesive forces. *Hum. Reprod.* **13**, 3211–3219 (1998).
72. Benoit, M. & Gaub, H. E. Measuring Cell Adhesion Forces with the Atomic Force Microscope at the Molecular Level. *Cells Tissues Organs* **172**, 174–189 (2002).
73. Puech, P.-H. Measuring cell adhesion forces of primary gastrulating cells from zebrafish using atomic force microscopy. *J. Cell Sci.* **118**, 4199–4206 (2005).
74. Puech, P.-H., Poole, K., Knebel, D. & Muller, D. J. A new technical approach to quantify cell–cell adhesion forces by AFM. *Ultramicroscopy* **106**, 637–644 (2006).
75. Cross, S. E. *et al.* AFM-based analysis of human metastatic cancer cells. *Nanotechnology* **19**, 384003 (2008).
76. Murray, P., Frampton, G. & Nelson, P. Cell adhesion molecules. *BMJ* **319**, 332–334 (1999).
77. Alberts, B. *et al. Molecular Biology of the Cell*. (Garland Science, 2002).
78. Delva, E., Tucker, D. K. & Kowalczyk, A. P. The Desmosome. *Cold Spring Harb. Perspect. Biol.* **1**, a002543–a002543 (2009).
79. Desai, B. V., Harmon, R. M. & Green, K. J. Desmosomes at a glance. *J. Cell Sci.* **122**, 4401–4407 (2009).
80. Gallicano, G. I. *et al.* Desmoplakin Is Required Early in Development for Assembly of Desmosomes and Cytoskeletal Linkage. *J. Cell Biol.* **143**, 2009–2022 (1998).

81. Najor, N. A. Desmosomes in Human Disease. *Annu. Rev. Pathol. Mech. Dis.* **13**, 51–70 (2018).
82. Thomason, H. A., Scothern, A., McHarg, S. & Garrod, D. R. Desmosomes: adhesive strength and signalling in health and disease. *Biochem. J.* **429**, 419–433 (2010).
83. Garrod, D. & Tabernero, L. Hyper-adhesion: A Unique Property of Desmosomes. *Cell Commun. Adhes.* **21**, 249–256 (2014).
84. Thiene, G., Corrado, D. & Basso, C. Arrhythmogenic right ventricular cardiomyopathy/dysplasia. *Orphanet J. Rare Dis.* **2**, 45 (2007).
85. Marcus, F. I. *et al.* Right ventricular dysplasia: a report of 24 adult cases. *Circulation* **65**, 384–398 (1982).
86. Corrado, D., Basso, C. & Judge, D. P. Arrhythmogenic Cardiomyopathy. *Circ. Res.* **121**, 784–802 (2017).
87. Marcus, F. I., Edson, S. & Towbin, J. A. Genetics of Arrhythmogenic Right Ventricular Cardiomyopathy. *J. Am. Coll. Cardiol.* **61**, 1945–1948 (2013).
88. Corrado, D. *et al.* Treatment of arrhythmogenic right ventricular cardiomyopathy/dysplasia: an international task force consensus statement. *Eur. Heart J.* ehv162 (2015). doi:10.1093/eurheartj/ehv162
89. Lombardi, R. & Marian, A. J. Arrhythmogenic right ventricular cardiomyopathy is a disease of cardiac stem cells: *Curr. Opin. Cardiol.* **25**, 222–228 (2010).
90. Thiene, G. & Basso, C. Arrhythmogenic right ventricular cardiomyopathy: An update$. *Cardiovasc. Pathol.* 9 (2001).
91. Peters, M. N., Katz, M. J. & Alkadri, M. E. Diagnosis of Arrhythmogenic Right Ventricular Cardiomyopathy. *Bayl. Univ. Med. Cent. Proc.* **25**, 349–353 (2012).
92. McKenna, W. J. *et al.* Diagnosis of arrhythmogenic right ventricular dysplasia/cardiomyopathy. Task Force of the Working Group Myocardial and Pericardial Disease of the European Society of Cardiology and of the Scientific Council on Cardiomyopathies of the International Society and Federation of Cardiology. *Heart* **71**, 215–218 (1994).

93. Marcus, F. I. *et al.* Diagnosis of Arrhythmogenic Right Ventricular Cardiomyopathy/Dysplasia: Proposed Modification of the Task Force Criteria. *Circulation* **121**, 1533–1541 (2010).

94. Turrini, P., Basso, C., Daliento, L., Nava, A. & Thiene, G. Is arrhythmogenic right ventricular cardiomyopathy a paediatric problem too? *Images Paediatr. Cardiol.* **3**, 18–37 (2001).

95. Pilichou, K., Basso, C., Corrado, D. & Thiene, G. Arrhythmogenic Cardiomyopathy. in *Diagnosis and Management of Adult Congenital Heart Disease* 631–639 (Elsevier, 2018). doi:10.1016/B978-0-7020-6929-1.00063-0

96. Gene therapy ac. Available at: https://techtransfer.universityofcalifornia.edu/NCD/29006.html. (Accessed: 20th November 2018)

97. Protonotarios, N. & Tsatsopoulou, A. Naxos disease and Carvajal syndrome. *Cardiovasc. Pathol.* **13**, 185–194 (2004).

98. Karmouch, J., Protonotarios, A. & Syrris, P. Genetic basis of arrhythmogenic cardiomyopathy: *Curr. Opin. Cardiol.* 1 (2018). doi:10.1097/HCO.0000000000000509

99. De Bortoli, M. *et al.* Whole-Exome Sequencing Identifies Pathogenic Variants in *TJP1* Gene Associated With Arrhythmogenic Cardiomyopathy. *Circ. Genomic Precis. Med.* **11**, (2018).

100. Poloni, G. *et al.* A targeted next-generation gene panel reveals a novel heterozygous nonsense variant in the TP63 gene in patients with arrhythmogenic cardiomyopathy. *Heart Rhythm* (2018). doi:10.1016/j.hrthm.2018.11.015

101. Hall, C. L. *et al.* Frequency of genetic variants associated with arrhythmogenic right ventricular cardiomyopathy in the genome aggregation database. *Eur. J. Hum. Genet.* **26**, 1312–1318 (2018).

102. McKoy, G. *et al.* Identification of a deletion in plakoglobin in arrhythmogenic right ventricular cardiomyopathy with palmoplantar keratoderma and woolly hair (Naxos disease). *The Lancet* **355**, 2119–2124 (2000).

103. Rampazzo, A. *et al.* Mutation in Human Desmoplakin Domain Binding to Plakoglobin Causes a Dominant Form of Arrhythmogenic Right Ventricular Cardiomyopathy. *Am. J. Hum. Genet.* **71**, 1200–1206 (2002).

104. Gerull, B. *et al.* Mutations in the desmosomal protein plakophilin-2 are common in arrhythmogenic right ventricular cardiomyopathy. *Nat. Genet.* **36**, 1162–1164 (2004).

105. Pilichou, K. *et al.* Mutations in Desmoglein-2 Gene Are Associated With Arrhythmogenic Right Ventricular Cardiomyopathy. *Circulation* **113**, 1171–1179 (2006).

106. Syrris, P. *et al.* Arrhythmogenic Right Ventricular Dysplasia/Cardiomyopathy Associated with Mutations in the Desmosomal Gene Desmocollin-2. *Am. J. Hum. Genet.* **79**, 978–984 (2006).

107. Siragam, V. *et al.* TMEM43 Mutation p.S358L Alters Intercalated Disc Protein Expression and Reduces Conduction Velocity in Arrhythmogenic Right Ventricular Cardiomyopathy. *PLoS ONE* **9**, e109128 (2014).

108. Merner, N. D. *et al.* Arrhythmogenic Right Ventricular Cardiomyopathy Type 5 Is a Fully Penetrant, Lethal Arrhythmic Disorder Caused by a Missense Mutation in the TMEM43 Gene. *Am. J. Hum. Genet.* **82**, 809–821 (2008).

109. Milting, H. *et al.* The TMEM43 Newfoundland mutation p.S358L causing ARVC-5 was imported from Europe and increases the stiffness of the cell nucleus. *Eur. Heart J.* **36**, 872–881 (2015).

110. Quarta, G. *et al.* Mutations in the Lamin A/C gene mimic arrhythmogenic right ventricular cardiomyopathy. *Eur. Heart J.* **33**, 1128–1136 (2012).

111. Kato, K. *et al.* LMNA cardiomyopathy detected in Japanese arrhythmogenic right ventricular cardiomyopathy cohort. *J. Cardiol.* **68**, 346–351 (2016).

112. Tewari, R., Bailes, E., Bunting, K. A. & Coates, J. C. Armadillo-repeat protein functions: questions for little creatures. *Trends Cell Biol.* **20**, 470–481 (2010).

113. Bonné, S., van Hengel, J., Nollet, F., Kools, P. & van Roy, F. Plakophilin-3, a novel armadillo-like protein present in nuclei and desmosomes of epithelial cells. *J. Cell Sci.* **112 (Pt 14)**, 2265–2276 (1999).

114. Chen, X., Bonné, S., Hatzfeld, M., van Roy, F. & Green, K. J. Protein Binding and Functional Characterization of Plakophilin 2: EVIDENCE FOR ITS DIVERSE ROLES IN DESMOSOMES AND β-CATENIN SIGNALING. *J. Biol. Chem.* **277**, 10512–10522 (2002).

115. Syrris, P. *et al.* Clinical Expression of Plakophilin-2 Mutations in Familial Arrhythmogenic Right Ventricular Cardiomyopathy. *Circulation* **113**, 356–364 (2006).

116. Neuber, S. *et al.* The Desmosomal Plaque Proteins of the Plakophilin Family. *Dermatol. Res. Pract.* **2010**, 1–11 (2010).

117. Calore, M., Lorenzon, A., De Bortoli, M., Poloni, G. & Rampazzo, A. Arrhythmogenic cardiomyopathy: a disease of intercalated discs. *Cell Tissue Res.* **360**, 491–500 (2015).

118. Corrado, D. *et al.* Relationship Between Arrhythmogenic Right Ventricular Cardiomyopathy and Brugada Syndrome: New Insights From Molecular Biology and Clinical Implications. *Circ. Arrhythm. Electrophysiol.* **9**, (2016).

119. Cerrone, M. *et al.* Missense Mutations in Plakophilin-2 Cause Sodium Current Deficit and Associate With a Brugada Syndrome Phenotype. *Circulation* **129**, 1092–1103 (2014).

120. Rickelt, S. *et al.* A novel kind of tumor type-characteristic junction: plakophilin-2 as a major protein of adherens junctions in cardiac myxomata. *Mod. Pathol.* **23**, 1429–1437 (2010).

121. Sweet, M. E., Taylor, M. R. & Mestroni, L. Diagnosis, prevalence, and screening of familial dilated cardiomyopathy. *Expert Opin. Orphan Drugs* **3**, 869–876 (2015).

122. Dellefave, L. & McNally, E. M. The genetics of dilated cardiomyopathy: *Curr. Opin. Cardiol.* **25**, 198–204 (2010).

123. Merlo, M. *et al.* Evolving concepts in dilated cardiomyopathy: Evolving concepts in DCM. *Eur. J. Heart Fail.* **20**, 228–239 (2018).

124. Lee, T. M. *et al.* Pediatric Cardiomyopathies. *Circ. Res.* **121**, 855–873 (2017).

125. Patel, M. D. *et al.* Pediatric and adult dilated cardiomyopathy represent distinct pathological entities. *JCI Insight* **2**, (2017).

126. Tatman, P. D. *et al.* Pediatric dilated cardiomyopathy hearts display a unique gene expression profile. *JCI Insight* **2**, (2017).

127. Maron, B. J. *et al.* Contemporary Definitions and Classification of the Cardiomyopathies: An American Heart Association Scientific Statement From the Council on Clinical Cardiology, Heart Failure and Transplantation Committee; Quality of Care and Outcomes Research and Functional Genomics and Translational Biology Interdisciplinary Working Groups; and Council on Epidemiology and Prevention. *Circulation* **113**, 1807–1816 (2006).

128. Hazebroek, M., Dennert, R. & Heymans, S. Idiopathic dilated cardiomyopathy: possible triggers and treatment strategies. *Neth. Heart J.* **20**, 332–335 (2012).

129. Mestroni, L. Guidelines for the study of familial dilated cardiomyopathies. *Eur. Heart J.* **20**, 93–102 (1999).

130. Lakdawala, N. K., Winterfield, J. R. & Funke, B. H. Dilated Cardiomyopathy. *Circ. Arrhythm. Electrophysiol.* **6**, 228–237 (2013).

131. Mestroni, L. & Taylor, M. R. G. Genetics and Genetic Testing of Dilated Cardiomyopathy: a New Perspective. 12 (2014).

132. McNally, E. M. & Mestroni, L. Dilated Cardiomyopathy: Genetic Determinants and Mechanisms. *Circ. Res.* **121**, 731–748 (2017).

133. Tskhovrebova, L. & Trinick, J. Titin: properties and family relationships. *Nat. Rev. Mol. Cell Biol.* **4**, 679–689 (2003).

134. Gerull, B. *et al.* Mutations of TTN, encoding the giant muscle filament titin, cause familial dilated cardiomyopathy. *Nat. Genet.* **30**, 201–204 (2002).

135. LeWinter, M. M. & Granzier, H. L. Cardiac Titin and Heart Disease: *J. Cardiovasc. Pharmacol.* **63**, 207–212 (2014).

136. Herman, D. S. *et al.* Truncations of Titin Causing Dilated Cardiomyopathy. *N. Engl. J. Med.* **366**, 619–628 (2012).

137. Linke, W. A. & Grützner, A. Pulling single molecules of titin by AFM—recent advances and physiological implications. *Pflüg. Arch. - Eur. J. Physiol.* **456**, 101–115 (2008).

138. Kass, S. *et al.* A gene defect that causes conduction system disease and dilated cardiomyopathy maps to chromosome 1p1–1q1. *Nat. Genet.* **7**, 546–551 (1994).

139. Fatkin, D. *et al.* Missense Mutations in the Rod Domain of the Lamin A/C Gene as Causes of Dilated Cardiomyopathy and Conduction-System Disease. *N. Engl. J. Med.* **341**, 1715–1724 (1999).

140. Nikolova, V. *et al.* Defects in nuclear structure and function promote dilated cardiomyopathy in lamin A/C–deficient mice. *J. Clin. Invest.* **113**, 357–369 (2004).

141. Goidescu, C. M. DILATED CARDIOMYOPATHY PRODUCED BY LAMIN A/C GENE MUTATIONS. *Clujul Med.* **86**, 4 (2013).

142. Cattin, M.-E., Muchir, A. & Bonne, G. 'State-of-the-heart' of cardiac laminopathies: *Curr. Opin. Cardiol.* **28**, 297–304 (2013).

143. Tesson, F. *et al.* Lamin A/C mutations in dilated cardiomyopathy. *Cardiol. J.* **21**, 331–342 (2014).

144. Modarres, H. P. & Mofrad, M. R. K. Filamin: A Structural and Functional Biomolecule with Important Roles in Cell Biology, Signaling and Mechanics. 28 (2014).

145. Stossel, T. P. *et al.* Filamins as integrators of cell mechanics and signalling. *Nat. Rev. Mol. Cell Biol.* **2**, 138–145 (2001).

146. Fujita, M. *et al.* Filamin C plays an essential role in the maintenance of the structural integrity of cardiac and skeletal muscles, revealed by the medaka mutant zacro. *Dev. Biol.* **361**, 79–89 (2012).

147. Feng, Y. & Walsh, C. A. The many faces of filamin: A versatile molecular scaffold for cell motility and signalling. *Nat. Cell Biol.* **6**, 1034–1038 (2004).

148. Brotschi, E. A., Hartwig, J. H. & Stossel, T. P. The gelation of actin by actin-binding protein. *J. Biol. Chem.* **253**, 8988–8993 (1978).

149. Leber, Y. *et al.* Filamin C is a highly dynamic protein associated with fast repair of myofibrillar microdamage. *Hum. Mol. Genet.* ddw135 (2016). doi:10.1093/hmg/ddw135

150. Begay, R. L. *et al.* FLNC Gene Splice Mutations Cause Dilated Cardiomyopathy. *JACC Basic Transl. Sci.* **1**, 344–359 (2016).

151. Valdés-Mas, R. *et al.* Mutations in filamin C cause a new form of familial hypertrophic cardiomyopathy. *Nat. Commun.* **5**, (2014).

152. Brodehl, A. *et al.* Mutations in *FLNC* are Associated with Familial Restrictive Cardiomyopathy. *Hum. Mutat.* **37**, 269–279 (2016).

153. Golbus, J. R. *et al.* Targeted Analysis of Whole Genome Sequence Data to Diagnose Genetic Cardiomyopathy. *Circ. Cardiovasc. Genet.* **7**, 751–759 (2014).

154. Reinstein, E. *et al.* Congenital dilated cardiomyopathy caused by biallelic mutations in Filamin C. *Eur. J. Hum. Genet.* **24**, 1792–1796 (2016).

155. Ortiz-Genga, M. F. *et al.* Truncating FLNC Mutations Are Associated With High-Risk Dilated and Arrhythmogenic Cardiomyopathies. *J. Am. Coll. Cardiol.* **68**, 2440–2451 (2016).

156. Sveinbjornsson, G. *et al.* Variants in *NKX2-5* and *FLNC* Cause Dilated Cardiomyopathy and Sudden Cardiac Death. *Circ. Genomic Precis. Med.* **11**, (2018).

157. Begay, R. L. *et al.* Filamin C Truncation Mutations Are Associated With Arrhythmogenic Dilated Cardiomyopathy and Changes in the Cell–Cell Adhesion Structures. *JACC Clin. Electrophysiol.* **4**, 504–514 (2018).

158. Corrado, D. & Zorzi, A. Filamin C. *JACC Clin. Electrophysiol.* **4**, 515–517 (2018).

159. Pollex, R. & Hegele, R. Hutchinson-Gilford progeria syndrome: Hutchinson-Gilford progeria syndrome. *Clin. Genet.* **66**, 375–381 (2004).

160. Carrero, D., Soria-Valles, C. & López-Otín, C. Hallmarks of progeroid syndromes: lessons from mice and reprogrammed cells. *Dis. Model. Mech.* **9**, 719–735 (2016).

161. Harhouri, K. *et al.* An overview of treatment strategies for Hutchinson-Gilford Progeria syndrome. *Nucleus* **9**, 265–276 (2018).

162. Hennekam, R. C. M. Hutchinson–Gilford progeria syndrome: Review of the phenotype. *Am. J. Med. Genet. A.* **140A**, 2603–2624 (2006).

163. Merideth, M. A. *et al.* Phenotype and Course of Hutchinson–Gilford Progeria Syndrome. *N. Engl. J. Med.* **358**, 592–604 (2008).

164. Nogueira, A. S. *et al.* Hutchinson-Gilford Progeria Syndrome (HGPS): relevant aspects of a rare syndrome diagnosed in a Brazilian child. *JORDI - J. Oral Diagn.* **1**, (2016).

165. progeria. Available at: https://www.progeriaresearch.org/progeria-101faq/, 20181017. (Accessed: 20th November 2018)

166. Strandgren, C., Revêchon, G., Carvajal, A. S. & Eriksson, M. Emerging candidate treatment strategies for Hutchinson-Gilford progeria syndrome. *Biochem. Soc. Trans.* **45**, 1279–1293 (2017).

167. Kim, H. K. *et al.* Hutchinson-Gilford Progeria Syndrome with G608G LMNA Mutation. *J. Korean Med. Sci.* **26**, 1642 (2011).

168. Gabr, M., Hashem, N., Hashem, M., Fahmi, A. & Safouh, M. Progeria, a pathologic study. *J. Pediatr.* **57**, 70–77 (1960).

169. Eriksson, M. *et al.* Recurrent de novo point mutations in lamin A cause Hutchinson–Gilford progeria syndrome. *Nature* **423**, 293–298 (2003).

170. De Sandre-Giovannoli, A. Lamin A Truncation in Hutchinson-Gilford Progeria. *Science* **300**, 2055–2055 (2003).

171. Kang, S., Yoon, M.-H. & Park, B.-J. Laminopathies; Mutations on single gene and various human genetic diseases. *BMB Rep.* **51**, 327–337 (2018).

172. Ahmed, M. S., Ikram, S., Bibi, N. & Mir, A. Hutchinson–Gilford Progeria Syndrome: A Premature Aging Disease. *Mol. Neurobiol.* (2017). doi:10.1007/s12035-017-0610-7

173. Ho, C. Y. & Lammerding, J. Lamins at a glance. *J. Cell Sci.* **125**, 2087–2093 (2012).

174. Pecorari, I., Puzzi, L. & Sbaizero, O. Atomic force microscopy and lamins: A review study towards future, combined investigations: Pecorari et al. *Microsc. Res. Tech.* **80**, 97–108 (2017).

175. Mounkes, L., Kozlov, S., Burke, B. & Stewart, C. L. The laminopathies: nuclear structure meets disease. *Curr. Opin. Genet. Dev.* **13**, 223–230 (2003).

176. Dittmer, T. A. & Misteli, T. The lamin protein family. *Genome Biol.* **12**, 222 (2011).

177. Skoczyńska, A., Budzisz, E., Dana, A. & Rotsztejn, H. New look at the role of progerin in skin aging. *Menopausal Rev.* **1**, 53–58 (2015).

178. Revêchon, G. *et al.* Rare progerin-expressing preadipocytes and adipocytes contribute to tissue depletion over time. *Sci. Rep.* **7**, (2017).

179. Dahl, K. N., Engler, A. J., Pajerowski, J. D. & Discher, D. E. Power-Law Rheology of Isolated Nuclei with Deformation Mapping of Nuclear Substructures. *Biophys. J.* **89**, 2855–2864 (2005).

180. Schäpe, J., Prauße, S., Radmacher, M. & Stick, R. Influence of Lamin A on the Mechanical Properties of Amphibian Oocyte Nuclei Measured by Atomic Force Microscopy. *Biophys. J.* **96**, 4319–4325 (2009).

181. Kaufmann, A., Heinemann, F., Radmacher, M. & Stick, R. Amphibian oocyte nuclei expressing lamin A with the progeria mutation E145K exhibit an increased elastic modulus. *Nucleus* **2**, 310–319 (2011).

182. Apte, K., Stick, R. & Radmacher, M. Mechanics in human fibroblasts and progeria: Lamin A mutation E145K results in stiffening of nuclei. *J. Mol. Recognit.* **30**, e2580 (2017).

183. Broers, J. L. V. *et al.* Decreased mechanical stiffness in LMNA−/− cells is caused by defective nucleo-cytoskeletal integrity: implications for the development of laminopathies. *Hum. Mol. Genet.* **13**, 2567–2580 (2004).

184. Lammerding, J. *et al.* Lamin A/C deficiency causes defective nuclear mechanics and mechanotransduction. *J. Clin. Invest.* **113**, 370–378 (2004).

185. Chen, S. N. *et al.* The Hippo Pathway Is Activated and Is a Causal Mechanism for Adipogenesis in Arrhythmogenic Cardiomyopathy. *Circ. Res.* **114**, 454–468 (2014).

186. Gurha, P., Chen, X., Lombardi, R., Willerson, J. T. & Marian, A. J. Knockdown of Plakophilin 2 Downregulates miR-184 Through CpG Hypermethylation and Suppression of the E2F1 Pathway and Leads to Enhanced Adipogenesis In Vitro. *Circ. Res.* **119**, 731–750 (2016).

187. Claycomb, W. C. *et al.* HL-1 cells: a cardiac muscle cell line that contracts and retains phenotypic characteristics of the adult cardiomyocyte. *Proc. Natl. Acad. Sci. U. S. A.* **95**, 2979–2984 (1998).

188. Proprietà meccaniche e biofisiche di singole cellule | Archivio della ricerca di Trieste. Available at: https://arts.units.it/handle/11368/2919797#.XACgzeInbIU. (Accessed: 30th November 2018)

189. Martinelli, V. *et al.* Carbon Nanotubes Promote Growth and Spontaneous Electrical Activity in Cultured Cardiac Myocytes. *Nano Lett.* **12**, 1831–1838 (2012).

190. Lanzicher, T. *et al.* AFM single-cell force spectroscopy links altered nuclear and cytoskeletal mechanics to defective cell adhesion in cardiac myocytes with a nuclear lamin mutation. *Nucleus* **6**, 394–407 (2015).

191. DNP-S10 - Bruker AFM Probes. Available at: https://www.brukerafmprobes.com/p-3256-dnp-s10.aspx. (Accessed: 25th February 2019)

192. CP-PNP-SiO AFM Probe - NanoAndMore. Available at: https://www.nanoandmore.com/AFM-Probe-CP-PNP-SiO. (Accessed: 25th February 2019)

193. PNP-TR-TL AFM Probe - NanoAndMore. Available at: https://www.nanoandmore.com/AFM-Probe-PNP-TR-TL. (Accessed: 25th February 2019)

194. Hecht, F. M. *et al.* Imaging viscoelastic properties of live cells by AFM: power-law rheology on the nanoscale. *Soft Matter* **11**, 4584–4591 (2015).

195. Puzzi Luca *et al.* Abstract 15489: Altered Biomechanical Properties of PKP2-deficient Hl-1 Cardiac Cells. *Circulation* **132**, A15489–A15489 (2015).

196. Kossivas, F. *et al.* Elasticity Measurements from Left Ventricular Murine HL-1 Cardiomyocytes using Atomic Force Microscopy. *FASEB J.* **29**, 799.8 (2015).

197. Rico, F. *et al.* Probing mechanical properties of living cells by atomic force microscopy with blunted pyramidal cantilever tips. *Phys. Rev. E* **72**, (2005).

198. Vargas-Pinto, R., Gong, H., Vahabikashi, A. & Johnson, M. The Effect of the Endothelial Cell Cortex on Atomic Force Microscopy Measurements. *Biophys. J.* **105**, 300–309 (2013).

199. Green, K. J., Getsios, S., Troyanovsky, S. & Godsel, L. M. Intercellular Junction Assembly, Dynamics, and Homeostasis. *Cold Spring Harb. Perspect. Biol.* **2**, (2010).

200. Bass-Zubek, A. E. *et al.* Plakophilin 2: a critical scaffold for PKCα that regulates intercellular junction assembly. *J. Cell Biol.* **181**, 605–613 (2008).

201. Dave, J. M. & Bayless, K. J. Vimentin as an Integral Regulator of Cell Adhesion and Endothelial Sprouting. *Microcirculation* **21**, 333–344 (2014).

202. Peña, B. *et al.* Injectable Carbon Nanotube-Functionalized Reverse Thermal Gel Promotes Cardiomyocytes Survival and Maturation. *ACS Appl. Mater. Interfaces* **9**, 31645–31656 (2017).

203. Verstraeten, V. L. R. M., Ji, J. Y., Cummings, K. S., Lee, R. T. & Lammerding, J. Increased mechanosensitivity and nuclear stiffness in Hutchinson–Gilford progeria cells: effects of farnesyltransferase inhibitors. *Aging Cell* **7**, 383–393 (2008).

204. Islam, M. *et al.* Microfluidic cell sorting by stiffness to examine heterogenic responses of cancer cells to chemotherapy. *Cell Death Dis.* **9**, (2018).

205. Liu, L. *et al.* Mechanoresponsive stem cells to target cancer metastases through biophysical cues. *Sci. Transl. Med.* **9**, eaan2966 (2017).

206. Andolfi, L. *et al.* Investigating the mechanical properties of zona pellucida of whole human oocytes by atomic force spectroscopy. *Integr. Biol.* **8**, 886–893 (2016).

207. Chan, C. K. *et al.* Tumour-suppressor microRNAs regulate ovarian cancer cell physical properties and invasive behaviour. *Open Biol.* **6**, 160275 (2016).

Acknowledgements

I would like to express my gratitude to my supervisor, Professor Orfeo Sbaizero, who gave me the greatest opportunity; I will not forget.

My acknowledgements are also devoted to the Professors I have worked with during these three years: Prof. Josè Luis Toca-Herrera and Dr. Jagoba Iturri, Prof. Ali J Marian, Prof. Luisa Mestroni, and Prof. Matt Taylor. Thanks for being part of my personal growth.

Sometimes, in your life, you meet people, and you do not realise immediately that they can become such a great source of inspiration. Raffaella and Suet Nee have made a lasting difference in my life, unconsciounsly becoming my mentors. They taught me more than what words can explain, and there is no better way to thank them than becoming the person they showed me I can be.

When you move around and work in different places, it can be difficult to establish true friendships. But, if you are lucky, one day you go at work and realise that your office-mates are more than two persons hanging around you for 8-12 hours a day. Alessia and Elisa are this kind of people. They are friends, and this thesis wouldn’t have been written without their great support.

I guess it is not because of fortuity that I will end this journey just one day before my friend Federica. We started together many years ago: two naive students, who were not able to hold back the laughter in class. We are now starting a new parenthesis of our life, and I am confident we will rock this, as usual.

To the people working at the B Building, who supported me with everything I needed, laughs and toasts.

To my friends, old and new: thanks for being part of my life. Simone, Andrea, Gabriele, Sergio, Emanuele, Milos & Petra, Cortney, Stefano, Valentina & Giorgio.

No blood ties could overcome what already exists between Massimiliano and me. I couldn’t ask for more than what you are already doing, as pretending to be my “big brother” and constantly believing in me.

To Valentina and Oreste, because I know that you were, you are, and you will always be by my side, no matter where I will end up.

For eight years now, I have tried to show to my little nephiew, Stefano, that being kind is always the right choice; that if you work hard, you will achieve great goals; that you must do your best to make the world a better place. Sometimes I was successful, sometimes not. My hope is that he will become the great man I glimpse in his eyes every time I look at him.

To my grandma, for teaching me the positive side of being stubborn.

In some families, passions are passed down from father to son. My grandpa and and my mom inspired me with their love for knowledge and their humbleness in trying to find a way to share this knowledge. This work is for you both.

Finally, my deepest gratitudine to those who always believed and encouraged me to pursue my dreams.